Hudson Valley Fog Environments

DAVID R. FITZJARRALD AND G. GARLAND LALA

Atmospheric Sciences Research Center, State University of New York, Albany, New York

(Manuscript received 24 February 1989, in final form 14 June 1989)

ABSTRACT

Observations of 14 cases of radiation fog in the Hudson River valley in New York State are presented. Our emphasis is to connect the fog prediction problem to mechanisms in the nocturnal boundary layer that influence heat and moisture balances. Surface layer and boundary layer fogs are distinguished by the difference in dominant terms in the saturation specific humidity deficit budget. Fogs that persist longer than approximately 30 minutes are most frequently thicker than 50 m. The ultimate depth to which the fog grows is shown to be determined by initial conditions at sunset and by subsequent evolution of winds in the nocturnal boundary layer, as well as by surface transports and radiative cooling. Estimates of the surface and boundary layer heat budget are presented. Two new phenomena are identified: 1) A jump in specific humidity occurring during the early evening transition that shortens the time required to reach surface layer saturation; and 2) along-valley jetlike winds with maxima near 100 m altitude are shown to be frequent and their occurrence is associated with a threshold value of the along-valley surface pressure gradient. Such jets appear to have an important influence on deep fog, increasing or decreasing its likelihood depending on the sign of heat and moisture advection they associate with.

1. Introduction

Radiation fogs only occur in supportive, predictable conditions, referred to here as *fog environments.* These environments are defined by vertical boundary layer temperature, humidity, and wind structure, radiative cooling rate profiles, horizontal heat and moisture transport, as well as the surface conditions. Heat loss occurs directly through clear-air radiative flux divergence and indirectly through turbulent transports operating near the radiatively cooled surface. Since advective terms are also sometimes important to the local cooling rate, regional wind circulations and temperature gradients may also be important. We report here observations of the environments for a number of Hudson valley radiation fogs, focussing on the problem of determining fog onset time and ultimate fog thickness. At Albany, New York (42.4°N, 73.5°W), the site of experiments presented here, radiation fogs occur most frequently within an hour or two of dawn on fair autumn nights (Meyer and Lala 1989). Even given what appear to be ideal conditions (light surface winds on clear nights with a large synoptic high pressure center nearby), however, some nights yield persistent fogs and others stay mostly clear, showing only patchy fogs at best. The aim of this paper is to connect the fog prediction problem to mechanisms in the nocturnal boundary layer that influence heat and moisture balances.

Albany, New York lies near the confluence of the Hudson and Mohawk rivers. To the north, the axis of the Hudson merges with the Champlain Valley to provide an approximately north–south channel extending nearly 500 km from the Atlantic to the Canadian border (Fig. 1). For part of this distance the Hudson–Champlain valley is paralleled by the Connecticut River valley. Both valleys are susceptible to occurrences of widespread radiation fogs. When seen in early morning satellite images, such fogs clearly outline the dominant river valleys in the northeastern United States (Fig. 2). Near Albany, the Hudson valley is approximately 30 km wide, with high ground on either side of the valley eventually rising 200–300 m above the river. It should not be surprising that local and regional wind systems along the river valleys can be important, particularly in the absence of strong synoptic effects, a characteristic of nights with radiation fog.

Low-level winds in the Hudson valley have been observed to be channeled north–south along the valley since the earliest times. The first record we find of the relationship between winds along the Hudson valley and fog occurrence is in Robert Juet's journal of the 1609 Henry Hudson voyage (reprinted in Lunny 1959). Hudson's ship, the *Half Moon,* arrived at the mouth of the river on 2 September 1609 and the expedition spent a month in exploration, reaching the northern limit of navigation, near the current location of Albany, New York, on 19 September. Juet recorded

Corresponding author address: David R. Fitzjarrald, Atmospheric Sciences Research Center, State University of New York at Albany, 100 Fuller Road, Albany, NY 12222.

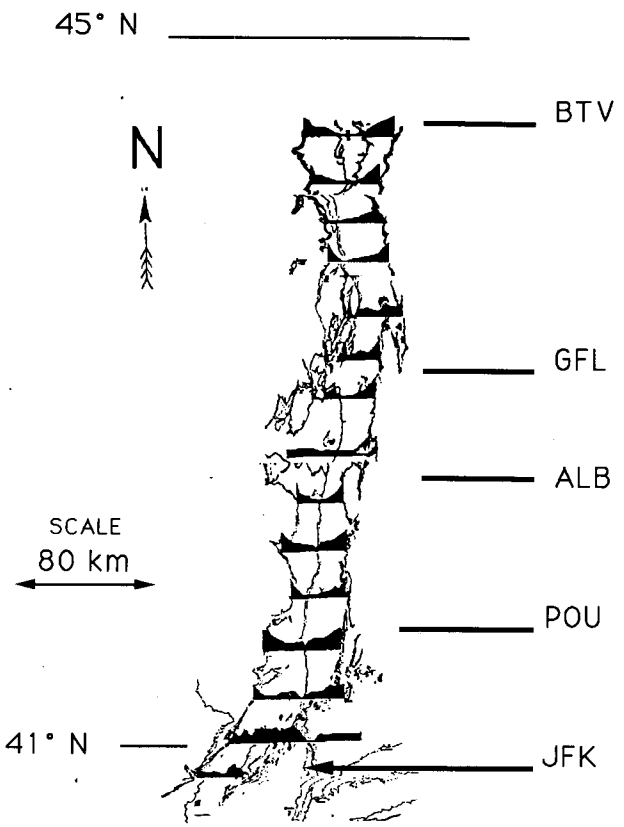

FIG. 1. The Hudson valley basin. Cross-sections to the 300 m level are shown in black. Stations along the valley identified by their synoptic codes are JFK (Kennedy Airport, New York City); POU (Poughkeepsie); ALB (Albany); GFL (Glens Falls); BTV (Burlington, VT). (Adapted from an original provided by W. Rodgers and R. Pilié, Calspan Corp.)

wind direction daily and commented occasionally on the weather during the trip. His journal indicates that Hudson was fortunate to have had nearly an unbroken four weeks of "faire weather" with which to conduct his explorations. We find the following remarks concerning the days 13–15 September 1609, when the ship was near the present location of West Point (41.2°N, 73.6°W):

> The thirteenth, faire weather, the wind Northerly. . . . The fourteenth . . . the wind South-east. . . . The fifteenth, in the morning was misty untill the Sunne arose; then it cleered. So wee weighed with the wind at South. . . .

The wind shifts during 13–15 September most probably corresponded to a pattern common to many autumnal fog episodes, with a surface high pressure center passing to the south, leading to the southerly wind that channels moist air up the valley. We report here on detailed observations made during the same season nearly 375 years later.

Six general, practical topics are central to any discussion of radiation fogs: 1) Fog onset time; 2) fog top growth and final fog thickness; 3) areal extent of fog; 4) internal fog dynamics; 5) visibility reduction and the microphysics of fog droplets; and 6) fog dissipation time. Here we address primarily the first three considerations, deferring discussion of fog microphysical observations and study of motions inside developed fogs to subsequent papers. In section 2 we review the field measurements relevant to this paper and discuss the techniques used to estimate terms in the surface heat budget. Based on our field experience, we formulate idealized models descriptive of the mechanisms we

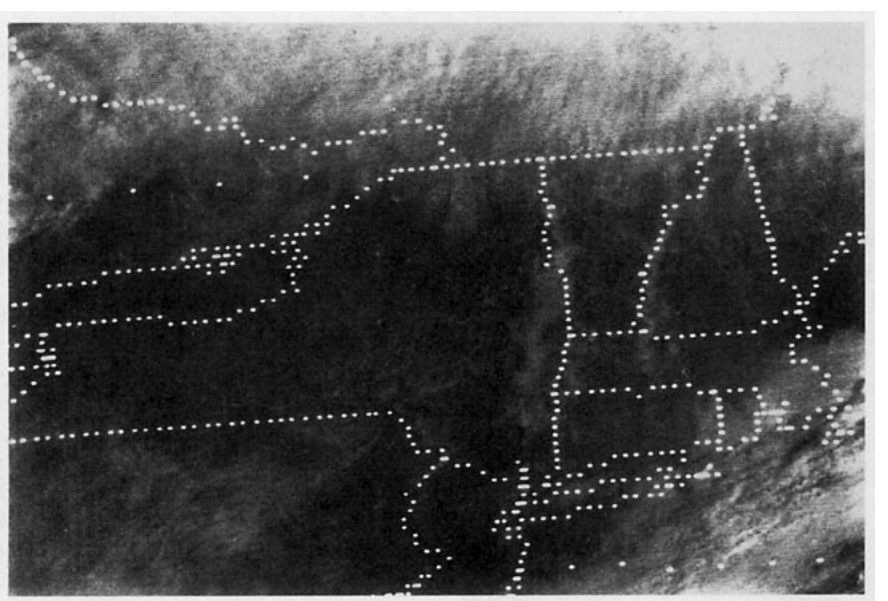

FIG. 2. GOES satellite image of New York and adjacent states, 1200 UTC 1 September 1982.

think are important in fog development (section 3) and then use our prototypes to describe fog environments seen at Albany, New York for five sequences during field experiments performed during the autumns of 1981 and 1982. We describe a series of case study periods (section 4) and discuss fog promoting mechanisms active during the case studies (section 5), assessing the adequacy of our conceptual models. To conclude (section 6) we suggest possible numerical and observational experiments to test our models. Since one aim of fog research is to improve forecasting schemes, we also offer suggestions for relating the present results to operational forecasting with routinely available data.

2. Background

a. Approach to saturation

Describing fog onset is an initial value problem. Thus, an important part of defining likely fog environments is to describe the initial condition. To understand when fog will form we must describe the approach to saturation in the surface and boundary layers. Taylor (1917) viewed fog formation in the surface layer as a competition between the effects of dew deposition and radiative cooling. His plot of dewpoint depression against temperature in the early evening at Kew, England was an early attempt to describe the fog environment. Taylor and others (e.g., Rodhe 1962) also noted that turbulent mixing could also prevent, delay, or enhance fog formation. More recently, models that included turbulent exchange and radiative cooling (Oliver et al. 1978; Welch et al. 1986; Musson-Genon 1987; Turton and Brown 1987, among others) featured rather complicated treatments of cloud microphysics and radiative cooling along with much simpler parameterizations of vertical turbulent exchange. Most of the modeling studies aim to reproduce some features of a few observed fog cases, but little attention has been directed toward the importance of initial conditions, arguably an equally important factor for fog prediction.

The time it takes for a layer to approach saturation for given initial conditions, compared to the length of night, is one measure of fog probability. We put the different influences leading to fog onset in perspective by considering the budget of the saturation specific humidity deficit, elaborating on the budget method presented in Peterssen (1940). Because the saturation specific humidity depends on temperature, the budget of saturation specific humidity deficit, $q_s - q$, where q_s is the saturation and q the observed specific humidity, includes contributions of the heat and moisture budgets. Explicitly, we write $\partial q_s/\partial t \approx (1/p)[de_s(T)/dT]\partial T/\partial t$, where e_s is the saturation vapor pressure and we assume pressure to be approximately constant. The factor in brackets is the Clausius–Clapeyron equation, $de_s(T)/dT = [\epsilon L_v/RT^2]e_s(T)$, where $\epsilon \approx 0.622$, L_v is the latent heat of vaporization of water, R the gas constant for dry air, and T the absolute temperature. The saturation and observed specific humidity budgets can be written:

Saturation specific humidity budget. . . .

$$\partial q_s/\partial t \approx (1/p)[de_s(T)/dT]\{\partial T/\partial t\}, \quad (1a)$$

where

$$\underset{1}{\partial T/\partial t} = \underset{2}{-\partial R_n/\partial z} \underset{3}{- \partial(wT)/\partial z} \underset{4}{- v_h\nabla_h T} \underset{5}{- W(\partial T/\partial z - \gamma)} \underset{6}{+ L_v(c - e)} \quad (1b)$$

Specific humidity budget. . . .

$$\underset{1}{\partial q/\partial t} = \underset{3}{-\partial(wq)/\partial z} \underset{4}{- v_h\nabla_h q} \underset{5}{- W(\partial q/\partial z)} \underset{6}{- (c - e)} \quad (2)$$

where notation is standard, except that R_n is the net radiation (in kinematic units), γ is the adiabatic lapse rate, v_h the horizontal wind vector, W the large-scale mean subsidence, and the term $L_v(c - e)$ represents the thermal effect of condensation (c) minus evaporation (e) with L_v the latent heat of condensation. We have written the explicit heat budget inside the Clausius–Clapeyron multiplier to emphasize that the importance of cooling in determining the approach to saturation depends on the temperature. Terms in each budget are 1) local change, 2) radiative flux divergence, 3) turbulent flux divergence, 4) horizontal advection, 5) drying or warming effects of large-scale subsidence, and 6) the net effect of condensation or evaporation. Term 6 is important to the prefog environment only if a significant number of aerosols are activated. It can be important to the understanding of the heat balance at the surface, where dew forms (see section 2b below), but is probably negligible above the surface. Taylor's "race" between dew deposition and cooling balances the surface layer integral of term 2, the net radiative flux divergence in the q_s equation and term 3, the turbulent flux divergences, the turbulent balances included by Rodhe (1962), Oliver et al. (1978) and others additionally considered term 3 in the q_s equation. In later sections we make estimates of some of the other terms that appear to be relevant to radiation fog formation at Albany.

b. Previous field observations

There have been relatively few radiation fog field programs. Few research projects have been comprehensive enough to observe all of the six budget terms in the saturation deficit budget. Radiative flux divergence in the surface layer was only measured directly by Funk (1960). Turbulent flux divergence through a deep layer was measured only in the Cardington experiments (Roach et al. 1982); in other cases for which Table 1 indicates turbulence measurements, they refer to surface layer observation only, made using surface layer similarity flux-gradient relations. Because of the need to have more observations available to modelers and theoreticians, we have chosen to present details of a large number of case studies. The 14 likely fog cases we draw on in this work add significantly to the total number of cases studied in detail to date (Table 1).

3. Observations and analysis techniques

The primary observing site was at the side of the east–west runway at the Albany County airport, a point approximately 3 km south of the Mohawk River, 9 km west of the confluence of the Mohawk and Hudson rivers. Details of instrumentation and data acquisition schemes as well as photographs and maps of the site are presented in Meyer et al. (1986). In addition to regularly reported data (synoptic charts, surface stations, and the Albany radiosonde launches at 0000 and 1200 UTC), we use vertical profiles of thermodynamic quantities from two additional nightly free balloon launches (A.I.R., Inc. Airsondes), wind vector and thermodynamic data from tethered balloon profiles, and anemometer and psychrometer data from six levels on a 16 m micrometeorological tower. A dense network of surface stations, the Portable Automated Mesonet (PAM), was also operated at 25 locations within a 15 km radius of the base site. Although our group modified the tethered balloon psychrometer to increase its ventilation rate, sensor time lags may still lead to differences in ascent and descent profiles. To make sequences of profiles more comparable, all profile data presented in this paper are from descents, done at approximately 1 m s^{-1}.

For the purposes of this paper, we identify fog with visual range measured either by the AEG-Telefunken MS04 (at 1.5 m altitude) or Wright and Wright Fog-15 forward scattering visibility sensors (at 1.5 and 10 m altitude). Unless otherwise noted, visual range data presented in this paper refer to the lower sensors. Our aim here is to discuss only the bulk features of fogs. Details of the microphysical measurements will appear in a later work from our group. During the 1985 campaign, we operated the same surface station with a smaller, 8 m tall tower, along with a Campbell Scientific single axis sonic anemometer at 1.5 m (rapid response w and T) and an EG&G Model 103 three-axis sonic anemometer (u, v, and w) at 3 meters. No tethered balloon soundings were made during the 1985 experiment. Data from the more extensive 1981 and 1982 experiments is the main data source for this work, but we use the direct turbulence measurements from 1985 for selected illustrations.

While we present estimates of the surface heat and moisture budgets below, we note that not only are nocturnal fluxes small, but also the tower site, located in a mowed field at the side of the airport runway, represents only one type of surface that makes up the regional mosaic of surface types, which includes both urban and forested areas. Consequently, while the mechanisms we identify for surface layer transport may have some generality, the representativity of the fluxes for the region remain uncertain, and the absolute values should serve as a guide to the range of values likely to be encountered. The average roughness length z_0 at the airport site was $(3.8 \pm 2.4) \times 10^{-2}$ m. The large value of the standard deviation of z_0 could not be associated with wind direction but its variation with wind speed

TABLE 1. Selected field experiments.

Study	Terms observed (×) or estimated (E)						Maximum height (m)	Number of cases
	1	2	3	4	5	6		
Fleagle et al. 1952	×	E	E				150	2
Funk 1960	×	×					10	8
Pilié et al. 1975a,b	×	×	E	E	E	×	300	8
Roach et al. 1976	×	×	E			E	20	3
Caughey et al. 1978	×						250	14
Findlater 1985	×	E	E				250	6
FOG82 Albany (Meyer et al. 1986)	×	×	×	E	E	×	400	22
FOG85 Albany (unpublished)	×	×	×			×	8	3
Musson-Genon 1987	×	×	E	×			300	1
Cardington stratus experiment: Roach et al. 1982 Caughey et al. 1982 Slingo et al. 1982 Caughey and Kitchen 1984	×	×	×	E	E	×	1000	3

is given by $z_0 = 4.9 \times 10^{-2} + 1.6 \times 10^{-2}\, u$ (m s^{-1}) for winds above 0.5 m s^{-1}.

We have estimated turbulent heat and moisture fluxes using three standard techniques. Direct measurements using the eddy correlation method were done during the 1985 experiment only. For the 1981 and 1982 data, we estimate the total turbulent heat flux from the residual from the surface heat balance, taking into account the soil heat flux and the observed net radiation. The third technique is to find the turbulent fluxes using the standard surface layer flux-gradient relations (Businger et al. 1971). There are instrumental difficulties, detailed below, with using each method for the light-wind, strongly stable conditions considered here.

The surface heat budget can be written

$$H + \mathrm{LE} = S - R_n, \tag{3}$$

where H and LE are the turbulent sensible and latent heat fluxes, respectively, S is the surface soil heat flux, and R_n is the net radiation. Net radiation was measured directly, and the soil heat flux was estimated from observations of soil temperature sensors at six levels in the following way: We found the heat budget in each soil layer using a smoothing spline to find the average value of $\partial T/\partial t$ in the soil and assumed the soil volumetric heat capacity to be 1.2×10^5 J m^{-3} K^{-1}, a value typical for the moist soil at the airport site. This estimate lies within experimental uncertainty of the value obtained from calorimetry techniques using soil samples taken from the same site during the 1985 experiment (C. Hsu, personal communication). The soil heat flux is probably not known better than to within 30%, and this estimate discounts the considerable inhomogeneity at the site. Although the ASRC net radiometer was not aspirated with dry air, it was dried hourly. Moreover, it agreed to within 2–4 W m^{-2} with a similar, aspirated net radiometer also operated at the base site (Ackerman et al. 1982). We have confidence that the net radiation measurement is reasonable when the dome is dry, and this is confirmed by the balance of the heat budget obtained during the dry morning hours (see below). The net radiometer dome becomes covered with dew during fog, and estimates of R_n then are not valid. It seems plausible that the value of net radiation under foggy conditions would be greatly reduced. When we estimate the total H + LE by the residual method, there are many sources of error, especially during the core of the night, when the residual comes as the smaller difference of two uncertain quantities. To the extent that errors are random, we can minimize their effect at the expense of having temporal resolution by averaging over long periods. Consequently, we present estimates made by this and by the profile method as long-term averages. One serious problem with this technique is that the soil heat flux depends linearly on the poorly known soil heat capacity, and this introduces a potential systematic error.

To split the total turbulent flux into its component parts before the air reaches saturation, one can estimate the relative size of sensible and latent contributions to their sum by appealing to the similarity forms of their profiles: the ratio of the fluxes (the Bowen ratio) should be equal to $L_v \Delta q / c_p \Delta T$, where L_v is the latent heat of vaporization of water and c_p is the specific heat at constant pressure for air. After the surface layer saturates, the Bowen ratio is simply a function of temperature and the temperature gradient. For conditions presented here, it varies approximately from 0.5 to 1.

Surface layer turbulent heat and moisture fluxes were estimated using observed profiles of temperature, wind speed, and humidity from the 16 m mast, applying the Obukhov similarity expression (Businger et al. 1971) for these profiles. Our estimates for stable conditions were done using a least-squares implementation of the technique described by Webb et al. (1970). Fluxes for convective conditions were found using an iterative method, applying standard flux-gradient formulas. The wind profile is poorly defined during very light wind conditions because of the anemometer threshold and hysteresis effects. That these effects can lead to significant wind speed underestimates was confirmed by the 1985 intercomparison between the sonic and Gill propeller anemometers. The average wind profile was observed not even to be monotonic for long periods during lulls. We salvaged flux estimates from gradients in the night using the following procedure: If the average wind speed fell below 0.1 m s^{-1} (an optimistic estimate of the threshold wind speed) during an averaging subperiod, or if the wind profile were not monotonic, fluxes were set to zero for that period. There was little difference in 2-hourly means of the fluxes if the subperiod was of 5 or 10 minute duration, and the latter was used. During the 1985 experiment, the directly measured heat flux was smaller than that estimated by the profile method when sufficient wind was present. For the most stable conditions, our estimates of the turbulent fluxes should be considered as only rough guides. One can assess the overall validity of the result by comparing the turbulent fluxes obtained by several different methods (see below).

The radiative flux profile was found using the Roach and Slingo (1979) five-band radiative transfer model. Vertical humidity and temperature profiles used as input to the model were interpolated in the vertical using data from the 16-m tower, the tethered balloon profiles, and airsonde or radiosonde data. The model levels were derived from a geometric progression of level separations in terms of pressure, resulting in 4 m resolution near the surface with a total of 100 levels below 300 mb. This version of the model has been compared with a broadband radiative transfer model (D. O. Starr, personal communication) for several fog cases. General agreement between the models is quite good, with differences in the calculated cooling rates less than 20 percent. These comparisons, along with those reported

by Roach and Slingo (1979) provide assurance that the model accuracy is satisfactory for our purposes.

3. Conceptual models

We find it convenient to distinguish *surface layer fogs,* whose environment is characterized by the dominant role that turbulence near the ground plays in the heat and moisture balances, from deeper *boundary layer fogs,* whose environment is strongly influenced by clear air radiative cooling and advective effects from local winds. Surface layer fogs typically are confined to a layer of strong stability no thicker than 20 m, two to four times the value of the nocturnal surface Obukhov length. At Albany, surface layer fogs usually precede boundary layer fogs, but their presence is only necessary, not sufficient for deeper boundary layer fogs to form. Shallow surface layer fogs are usually characterized by intermittent visual range observations.

Boundary layer fogs, observed to extend no higher than 150 m at Albany, are present develop differently if they are primarily thermodynamically driven by cooling in place or if the nocturnal boundary layer dynamics is also important. Another distinction is between fogs that actively modify winds in the boundary layer, both thermodynamically and dynamically, and those that appear to act passively as tracers of existing boundary layer flows.

a. *Surface layer model*

Because of observational convenience and their practical importance to transportation, surface layer fogs have been most extensively studied. The tension between the effects of surface layer cooling and moisture deposition is frequently cited as the central question in surface fog studies. Oliver et al. (1978) present a modern similarity interpretation of Taylor's (1917) criterion for existence of turbulence-dominated surface fogs. They concluded that turbulent heat fluxes can dominate radiative cooling in layers deeper than a few meters only in the presence of appreciable winds. We have noted another important phenomenon that influences the onset of surface fogs: Moisture convergence that occurs during the *early evening transition* from convective to stable conditions in the surface layer reduces the time for the layer to reach saturation. Three periods we consider in surface fog formation are: 1) early evening transition, 2) dew deposition and intermittent turbulence, and 3) surface layer response to deep fogs.

1) Early evening surface layer transition

Two examples illustrate the early evening transition (Fig. 3). The more typical example, Fig. 3a, shows an increase in q coincident with the rapid decline in mechanical mixing, as evidenced by the σ_w trace. On 25 September (Fig. 3b), a period of enhanced winds near 2000 LST led to a repetition of the transition. Accordingly, two jumps in specific humidity, one just before 1800 LST and one just before 2100 LST, are seen. In Fig. 3b, we note that between 1800 and 1900 LST the heat budget does not balance ($S - R_n = H + \mathrm{LE}$), and we attribute this to the difficulty of obtaining reasonable fluxes from profiles during this period. We observed such a jump in q in all but 1 of the 14 cases presented here. A physical explanation for the q jump may be as follows: After σ_w decreases below some value, rapid cooling occurs and $\partial q_s/\partial t$ becomes large. With waning shortwave radiation in the late afternoon, net radiation increases rapidly during the transition and then decays slowly after the mechanical turbulence decays. (We take upwards to be positive for all fluxes.) Turbulent heat flux becomes relatively strongly negative until eddy motions are finally damped out by steadily increasing surface layer stability. This leads to an early-evening maximum in the downward sensible heat flux (Fig. 3a), a phenomenon also observed by Caughey et al. (1979, their Fig. 13) and presented as an anomaly by Turton and Brown (1987, their Fig. 4). Wyngaard (1975) also modeled this negative sensible heat flux pulse using second-order closure.

During this initial period of turbulence-dominated transport, moisture flux is normally still positive. The 1985 eddy-correlation turbulent fluxes in the transition period (Table 2) confirm that not only are the heat and moisture fluxes in opposite directions, but also that the Obukhov length (L) generally decreases during the transition period, a feature also obtained in the Wyngaard (1975) and Brost and Wyngaard (1978) model results, indicating that mechanically driven turbulence ceases at some level not too far above the surface. Many of our cases show a protracted period of upward latent and downward sensible heat flux. If, in addition to positive q flux, the stable surface layer decouples from the boundary layer above at some height (as values of L in Table 2 would lead one to infer), turbulent moisture flux convergence can coincide with heat flux divergence in the surface layer. Flux convergence leads both to a jump in specific humidity and an abrupt drop in temperature, each effect diminishing the initial saturation deficit to be overcome before fog can form.

To determine the likely time of a moisture jump, we must describe the decay of mechanical turbulence in the surface layer. Although direct measurements of the turbulent eddy fluxes are not routinely available, the likely time when the moisture jump may occur may be seen in the surface layer temperature trace, commonly available at standard climatological stations. The period of turbulence-dominated cooling and moistening and the later period of radiatively dominated cooling are distinguished by a sign change in the mean *temporal curvature* of the surface-layer temperature. Supposing advection terms to be small and assuming conditions of horizontal homogeneity, inte-

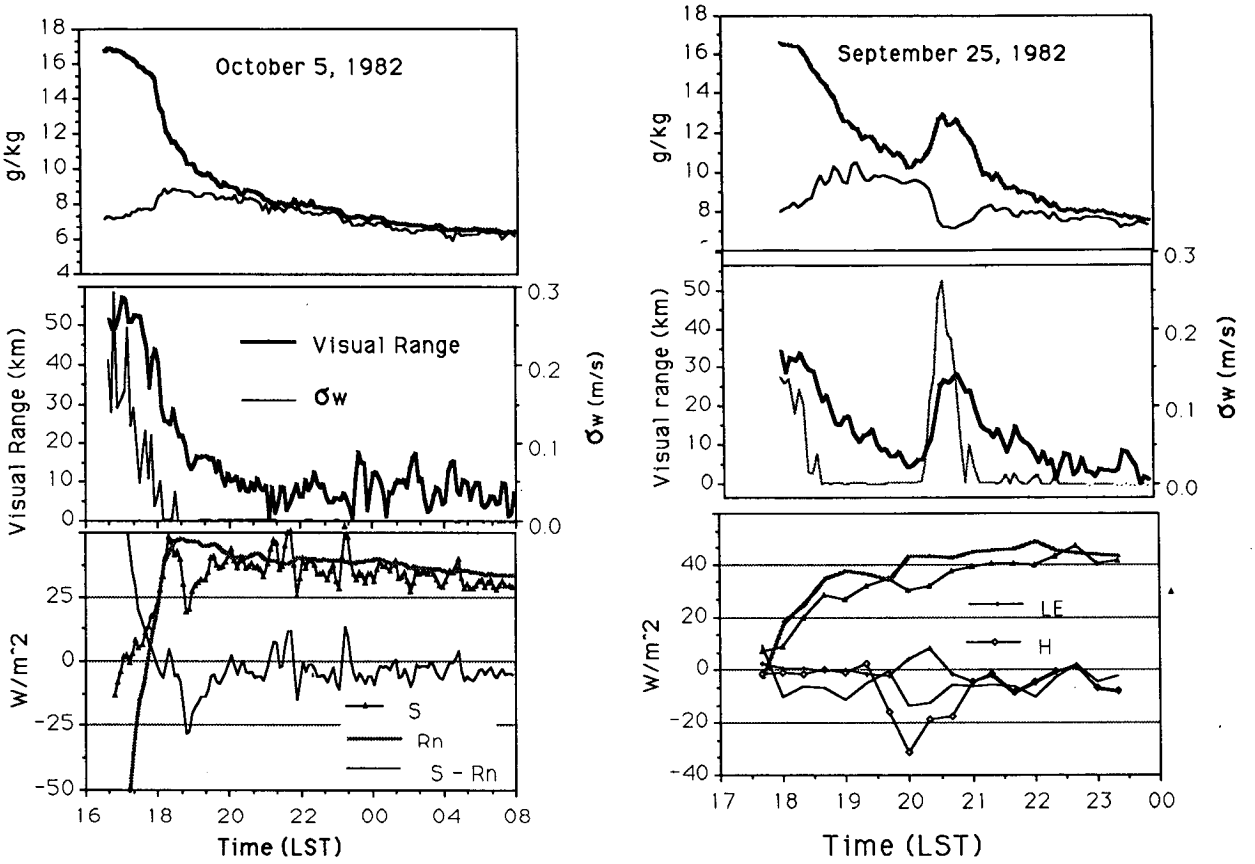

FIG. 3. (a) Surface observations made on 5 October 1982. Top panel: q_s (heavy solid line) and q (solid line). Center panel: Visual range and σ_w at 8 m. Bottom panel: Soil heat flux (S), net radiation (R_n), and the residual ($S - R_n$). (b) Same as (a) for 25 September 1982. Additional traces in the bottom panel are turbulent fluxes obtained using the profile method are the sensible heat flux (H) and the latent heat flux (LE).

grating (1b) from the surface to z_s, a height at which turbulent transports are small, and taking the time derivative yields the following expression for the layer-averaged temporal curvature:

$$z_s \partial^2 T/\partial t^2 = \partial/\partial t(w\theta_0 - w\theta_s) + \partial/\partial t(R_{n0} - R_{ns}),$$

where subscripts 0 and s refer to $z = z_0$, and $z = z_s$. If we place z_s at the lowest level of zero heat flux, then $w\theta_s$ can be ignored. Above this level, we can plausibly assume for the short term that the heat and moisture profiles do not change appreciably, and that changes in the downwelling radiation would also be small. Model results indicate that changes in upwelling radiative flux are also likely to be small above the surface, and during the early-evening surface layer transition, we ignore R_{ns} in comparison to the surface term:

$$z_s \partial^2 T/\partial t^2 \approx \partial w\theta_0/\partial t + \partial R_{n0}/\partial t.$$

It is clear that the first term on the right side is initially negative, changes to positive and then returns to near

TABLE 2. Early evening surface layer transition.

Time (LST)	u_8 (m s^{-1})	σ_{w1} (m s^{-1})	σ_{w2} (m s^{-1})	σ_T (K)	$\overline{wT}$ (10^{-2} K m s^{-1})	$\overline{wq}$ [10^{-2} (g kg^{-1}) m s^{-1}]	L (m)
1657	1.38	0.11	0.13	0.24	−0.65	0.68	24.2
1718	1.45	0.11	0.13	0.23	−0.81	0.61	27.6
1737	0.52	0.06	0.08	0.23	−0.39	0.11	9.8
1757	0.23	0.04	0.06	0.38	−0.17	0.07	7.3
1817	0.11	0.04	0.07	0.38	−0.27	0.09	4.3
1857	0.20	0.04	0.05	0.36	−0.37	0.24	2.9
1937	0.29	0.04	0.05	0.37	−0.10	−0.28	7.8
1957	0.16	0.04	0.04	0.25	−0.04	0.11	23.0

zero as mechanical turbulence decays. The second term is positive, changing to a small negative value after the transition. Thus, one expects the inflection point in the temperature (or q_s) trace to occur not long after the time of maximum downward flux. The changes in curvature of the temperature trace and the jump in specific humidity are indeed observed to occur during the period when turbulence, as measured σ_w, has fallen to near zero (an example is given in Fig. 3), though the apparent period of enhanced downward sensible heat flux, obtained as a residual from differencing the net radiative and soil heat fluxes occurs later (Fig. 3b). Since this feature is not specific to fog formation, we are currently performing more complete observational confirmation of this feature based on other surface layer observations, and this will be reported later. During the remainder of the evening, the relation indicates that the curvature will approach zero, and $\partial T/\partial t$ should be nearly constant with time, as is also observed. The curvature technique provides a simple way to identify the early-evening transition in routinely available data from surface climate stations.

Note that the q jump compensates for nearly six hours of the subsequent slow decay in specific humidity, presumably caused by dew formation. Although dew deposition tends to reduce fog likelihood (Taylor's 1917 argument), surface layer specific humidity does not drop fast enough in Albany fogs to delay the initial period of apparent saturation appreciably. To avoid the q surge from upsetting simple forecast techniques such as Taylor's, one must make the initial observation well after the surface layer transition is complete. Reference to the curvature in the temperature trace may aid in locating the transition.

2) Dew deposition and the nocturnal heat budget

After the initial period of rapid cooling and moistening, turbulent processes become intermittent, and the surface layer cools at a rate determined by the radiative flux divergence and the occasional coupling with the surface. We expect that soil heat flux and net radiation near the surface to be nearly in balance after the early evening transition. The surface moisture flux required to account for the observed $\partial q/\partial t$ can be crudely estimated by assuming no moisture flux above approximately 15 m, the height to which a strong surface temperature inversion was most frequently seen. The dew rate estimates obtained by this method are smaller than dew plate estimates (Table 3) made both by our group and by collaborators at Calspan Corp. during the 1982 field phase for a variety of surrogate surfaces including "artificial grass" (Pilié et al. 1982). Note that similar dew estimates from the plates were found on nearly all occasions, including cases for which $\partial q/\partial t$ was small or nonexistent in the early evening. The size and sign of the difference between the two estimates can be explained by 1) noting that the emissivity of the dew plates may be larger than that of the ambient vegetation, cooling the plate and enhancing condensation; 2), along with Aitken (1885) and Monteith (1956), observing that dew consists both of turbulent diffusion from the air and distillation from the soil, or 3) that the moisture comes from a layer deeper than 15 m.

The loss of moisture from the air to dew can also be estimated by inferring the latent heat flux for the surface heat balance method or the gradient method. As may be expected from the earlier discussion of potential errors in estimating the heat balance, the nocturnal heat balance is not balanced observationally (Table 3). Gradient estimates of the latent heat flux are generally smaller than those from the dew plate and larger than $15\partial q/\partial t$. The gradient estimates of H + LE are generally larger than the residual $S - R_n$ from soil heat flux and net radiation. For the observed surface layer drying rate to balance the gradient moisture flux, the vapor must converge through a layer perhaps 30

TABLE 3. Surface layer heat and moisture budgets.

Date	q Jump at transition (g kg^{-1})	Budget estimates (W m^{-2}) 2000–0200 LST averages								$\partial\bar{q}/\partial t$ (g kg^{-1} h^{-1})	Dew plate accumulation (g m^{-2} h^{-1})
		H	LE	S	R_n	H + LE	$S - R_n$	Dew plate LE	15 $\partial\bar{q}/\partial t$		
8/9 Sep	+1	−28	−4	37	51	−32	−14	−10	~0	~0	14
9/10 Sep	+1.5	−4	−5	37	40	−9	−3	−18	−4	−0.30	18
25/26 Sep	NA	−8	−3	38	45	−11	−7	−15	−3	−0.23	21
30 Sep/1 Oct	+1	−7	−10	34	39	−17	−5	−11	−4	−0.30	16
2/3 Oct	+0.5	−14	−10	47	56	−24	−9	−13	−3	−0.20	19
5/6 Oct	+2	−1	−1	33	44	−2	−11	−10	−4	−0.30	15
6/7 Oct	+3	−12	−12	35	39	−24	−5	−11	−3	−0.23	16
10/11 Oct	+1	−6	−4	52	59	−10	−7	−14	−2	−0.16	20
12/13 Oct 1981	+1	—	—	—	—	—	—	−11	−2	−0.30	16
13/14 Oct 1981	+1	—	—	—	—	—	—	−11	−2	−0.14	16
27/28 Oct	0	−6	−5	33	48	−11	−15	−11	−4	−0.30	15
28/29 Oct	+1	−4	−3	26	39	−7	−13	−1	−1	−0.1	2

m thick. It appears reasonable to conclude that after the transition period is completed, H in the prefog environment is probably near -10 W m^{-2}, and LE is a similar value. Total turbulent cooling should be between -5 and -25 W m^{-2}. Dew plate measurements appear to overestimate the moisture flux from the air by 50 to 100 percent.

The approach to saturation in the surface layer is occasioned by sporadic lulls that lead to brief periods of rapid cooling and reduced visibility, as aerosols grow in response to the increased relative humidity. When the surface layer is shallow enough, gusts can warm the layer and increase visibility. This is one reason that persistent fogs in Albany are nearly always thicker than 50 m. After saturation is reached, moisture deposition keeps pace with falling saturation specific humidity. During the 1985 experiment, we measured w and T fluctuations directly. During the periods of light winds preceding fog, we observed (Fig. 4a) periods of rapid cooling to be associated with occasional lulls. Local patches can approach saturation even without calling on the mechanism of pooling cold air in low areas.

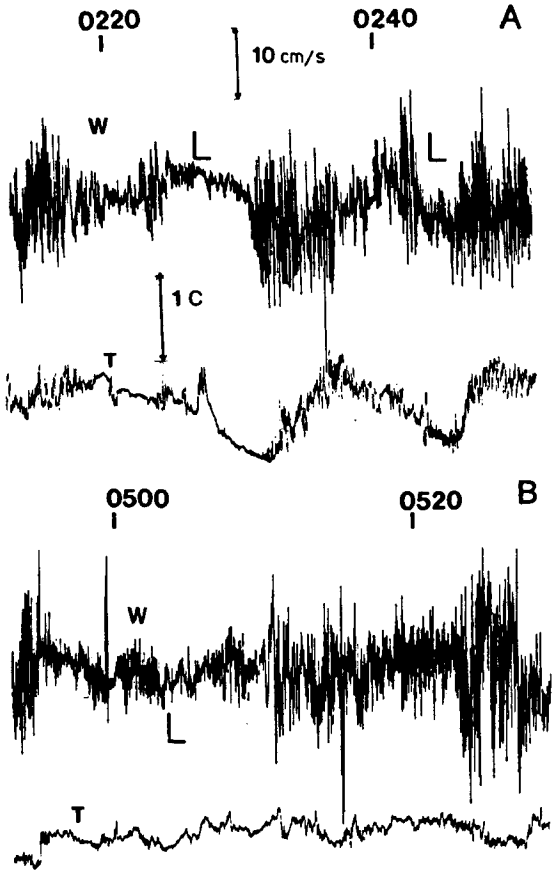

FIG. 4. Chart record traces from fast-response instruments of vertical velocity (w) and temperature (T) fluctuations observed at 1.5 m on 22/23 October 1985. A) Prefog environment: an example of lulls (designated by "L") under clear-sky conditions. B) Reduced temperature variance during a fog episode.

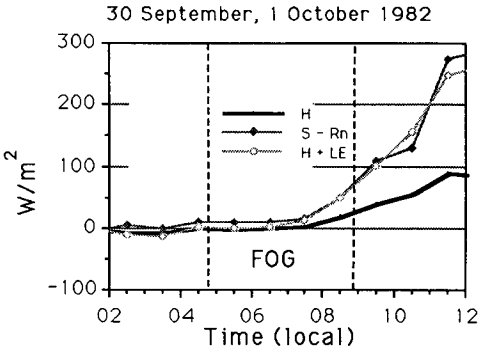

FIG. 5. Heat budget during and after fog on the morning of 1 October 1982.

Once fog forms, the surface layer stability decreases, and the level of maximum cooling leaves the ground, and the surface layer no longer exerts the dominant control on fog growth. Although mechanical mixing still occurs intermittently, it no longer causes temperature excursions (Fig. 4b). Soil heat flux continues, and the nearly neutral conditions that result have one important consequence: communication between the deeper fog layer and the surface layer. As a result, we suggest that microphysical observations, for example, made within the surface layer reflect processes occurring at higher levels during this period. Many fogs persist or grow after sunrise, depending on how close the boundary layer comes to saturation. An example (Fig. 5) shows the estimated surface heat budget as a nocturnal fog grew after sunrise, coexisting with sensible heat fluxes up to approximately 30 W m^{-2}. We show below that the fog grew appreciably thicker after dawn.

b. Boundary layer thermodynamic model

Hypothesizing that conditions in the boundary layer are, to a first approximation, evolving independently of those very near the surface, we can make a very simple, preliminary estimate of fog onset time in the boundary layer by assuming q to be constant with time. This assumption neglects to the first approximation dew deposition, only likely to be appreciable in the surface layer (Oliver et al. 1978); it agrees well with observations above 20 m made during the field experiment, with $\partial q_s/\partial t \gg \partial q/\partial t$. Many cases resemble the example presented in Fig. 6a. In the absence of significant horizontal advection and with a mean total cooling rate, $\partial T/\partial t$, the time it takes for fog to form is given by integrating the relation:

$$\partial(q_s - q)/\partial t \approx \partial q_s/\partial t \approx [\epsilon L_v/RT^2]q_s\partial T/\partial t, \quad (3)$$

from the initial saturation specific humidity, q_{s0}, to the final saturation value, namely q_0, the early evening value of the specific humidity. We note that the function $1/T^2$ varies only approximately 10% over the range of temperatures encountered when fog occurs

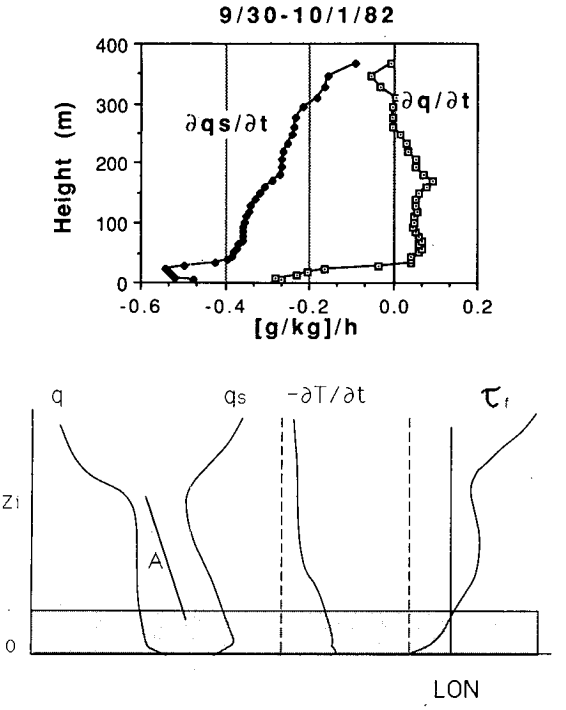

FIG. 6. (a) Rates of change of saturation specific humidity (q_s) and specific humidity (q) obtained by differencing tethered balloon soundings. (b) Schematic illustration of idealized thermodynamic conditions in the boundary layer in early evening. The height of the afternoon convective boundary layer (z_i), at approximately 1500 m altitude, and the length of the night (LON) are identified.

and hold it constant during the time integration of (3). This results in a relation between the time it takes to reach saturation, τ_f, the relative humidity at the start ($q_0/q_{s0} = \mathrm{RH}_0$), and the total cooling rate, $\partial T/\partial t$:

$$\tau_f \approx \ln(\mathrm{RH}_0)[(\epsilon L_v/RT^2)\partial T/\partial t]^{-1}, \qquad (4)$$

The local net cooling rate, Eq. (1), was assumed to be approximately constant during the time integration. If τ_f exceeds the length of night, then fog is unlikely. Equation (4) has proved useful for identifying climatological fog seasons at Albany (Meyer and Lala 1989).

As a conceptual model, consider the following prototype (Fig. 6b) of the boundary layer thermodynamic state at dusk, as the surface heat flux crosses zero as it changes from the positive daytime values to negative nighttime values: A convective boundary layer (CBL) grown during the day typically leads to formation of a well-mixed layer in q and in potential temperature, with the adiabatic temperature lapse reflected in the lapse of q_s. With q mixed and q_s dropping off, the relative humidity increases with height above the surface layer. Imposing a typical total cooling rate profile as given in the figure, one arrives at a profile of τ_f, small near the surface where both turbulent cooling and radiative flux divergence are largest reaching a maximum at the top of the surface layer. The low-level total cooling maximum is included in the schematic to recognize the role of turbulent cooling in that layer. For fog to form above the surface layer, the boundary layer must be moist enough initially and not suffer appreciable dry advection overnight. In principle, a second relative minimum could occur at the maximum afternoon height of the convective boundary layer, leading to small τ_f at the maximum height of the afternoon convective boundary layer. Possible appearance of a transient stratus deck there provides another mechanism to prevent fog from forming, as longwave cooling near the ground would thereby be reduced. This scenario did not occur in our cases, however, possibly because large-scale subsidence was too large.

Since surface moisture fluxes over land usually become small at night, the initial RH_0 that determines τ_f in the boundary layer is the result of afternoon convective mixing. Thus, the likelihood of saturation throughout the stable boundary layer depends strongly on events (for example, CBL growth and moistening) that occur on the afternoon preceding fog rather than on existing conditions at sunset or evolution of surface boundary conditions during the night. This indicates that soil moisture, for example, should correlate with deep fog likelihood because of moisture delivered to the atmosphere during the afternoon. Small fluxes that occur on the fog night are relatively less important.

c. *Local wind model*

Inland radiation fogs occur most frequently in valleys; to ignore channeling effects and local winds is to neglect an important part of the problem. Winds in river valleys are frequently observed to be channeled along the valley axis. Gross and Wipperman (1987) have demonstrated this effect convincingly in the wide, upper Rhine valley in Germany, and there is every reason to believe that similar flows occur in the Hudson valley. When there is a significant along-valley pressure gradient (strong cross-valley geostrophic wind component), the effect of valley sidewalls is to produce a small cross-valley pressure gradient that opposes the Coriolis force. This mechanism acts in concert with daytime turning toward lower pressure that friction associated with the convective boundary layer alone can accomplish. Samson et al. (1975) presented wind roses demonstrating that the predominant surface winds in the daytime follow the Hudson valley axis at Albany. At night, one expects frictional effects to diminish in importance. The Coriolis acceleration then might plausibly be balanced by cross-valley pressure gradients induced by a tilt in the thickness of a cooler, denser layer near the surface. Nocturnal stable layers are typically much shallower than the afternoon convective layer, and one expects the layer of along-valley motion to be shallower at night than in the day.

Observations lead us to consider three important dynamic layers in the Hudson valley nocturnal bound-

ary layer: 1) A stable surface layer, in which turbulent activity is presumed intermittent, reaching approximately to 20 m and underlying 2) a boundary layer in which channeling can occur if the pressure gradient along the valley is large enough. The second layer reaches approximately to 150 m, blending into 3) a region in which the wind direction is close to that of the synoptic scale geostrophic wind. Observations indicate that after only a few hours, less time than the 18 hour inertial period at Albany, winds at 250 m altitude correspond well to those at 850 mb. We hypothesize that residual convective turbulence in the CBL may be sufficient to couple the lower parts of the remnant CBL to the flow aloft after surface support for the CBL disappears, in the manner suggested by Nieuwstadt and Brost (1986). A schematic of the hypothesized form of the three layers is shown in Fig. 7. By exerting control on vertical relative humidity profile, advection in this layer can determine the maximum fog height. Rotation toward the westerly geostrophic flow at 850 mb usually brings in dry, potentially warm air during the autumn. Dynamical maintenance of channeled, moist southerly flow in the boundary layer can prevent dry westerly advection from deterring fog onset. Thus, it is conceivable that fairly strong boundary-layer winds up the valley could actually promote rather than inhibit fog formation, and we present an example of this in case 1 below. In the next section, we interpret sequences of observed q and q_s, using the conceptual wind and thermodynamics models as guides, and discuss elements of the saturation deficit budget.

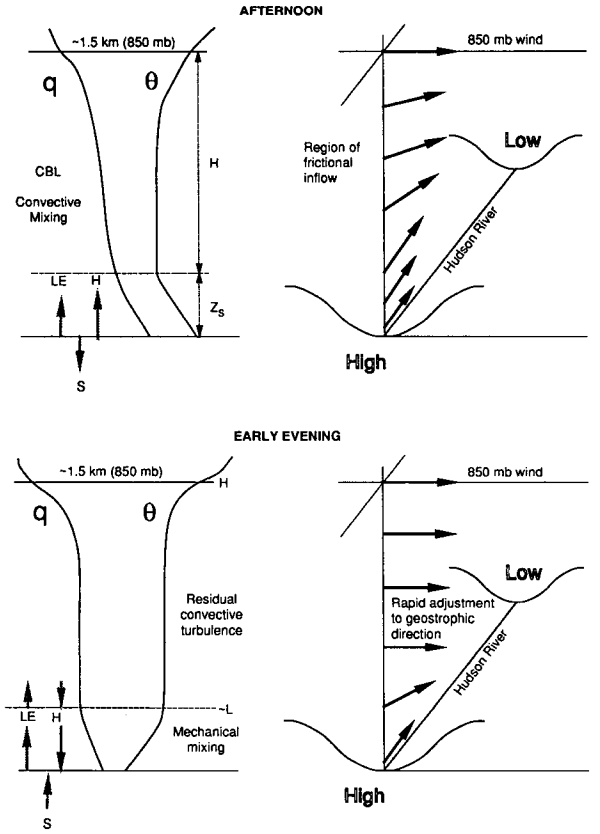

FIG. 7. Schematic comparison of boundary layer profiles in the afternoon and the early evening for the Hudson valley.

4. Case study periods

The conceptual models are hypotheses based on inferences made after analysis of a large number of individual fog events. No single event exhibits all features of the conceptual model. In this section we present a subset of the events considered as case studies, each of which validates some of the features described in the conceptual models. When possible, the case studies are arranged in series of consecutive days so that the fog environment on each night can be considered as partially deriving from the changing synoptic conditions. These cases show that in many instances significant thermodynamic changes in the lowest 200 m of the atmosphere occur on nights with low surface winds and weak synoptic scale pressure gradients. These thermodynamic changes are often related to ambient humidity in the CBL and the low-level wind structure along the Hudson river valley. Thus, it makes more sense to discuss the fog environment from the "top down," noting the position of the synoptic high pressure center, the thickness and humidity of the CBL, the sequence of soundings seen in the nocturnal stable boundary layer. In particular, we wish to illustrate how changes in the stable boundary layer winds during the night have a strong influence on the potential for deep fogs to form. We wish to emphasize that the boundary layer soundings are data unique to these case studies and are not currently routinely available to the forecaster, and that current operational data gives little information about these winds.

Sufficient data for detailed analysis are available for the six potential radiation fog periods during the 1981 and 1982 field campaigns. At the ground, these periods include four nights with persistent fog (measured visibility < 1 km for more than an hour continuously), six nights with patchy fog, and two nights with no fog. Standard plots (e.g., Fig. 8a) for each night of interest include: the surface pressure chart at 0700 LST on the morning following the case study night, a graph of potential temperature, specific humidity and winds up to 700 mb obtained from the Albany radiosonde with two additional airsonde launches made during the night, and the sequence of tethered balloon profiles of humidity and wind in the lowest 400 m. To identify foggy periods, time series of surface visual range (e.g., Fig. 8c) from the AEG device complement these data. Each case spans the period from the evening of the first day to the morning of the following day. Although we do not have direct measurements of the presence of fog above the surface layer, we refer to fog thickness as the depth through which the psychrometer on the

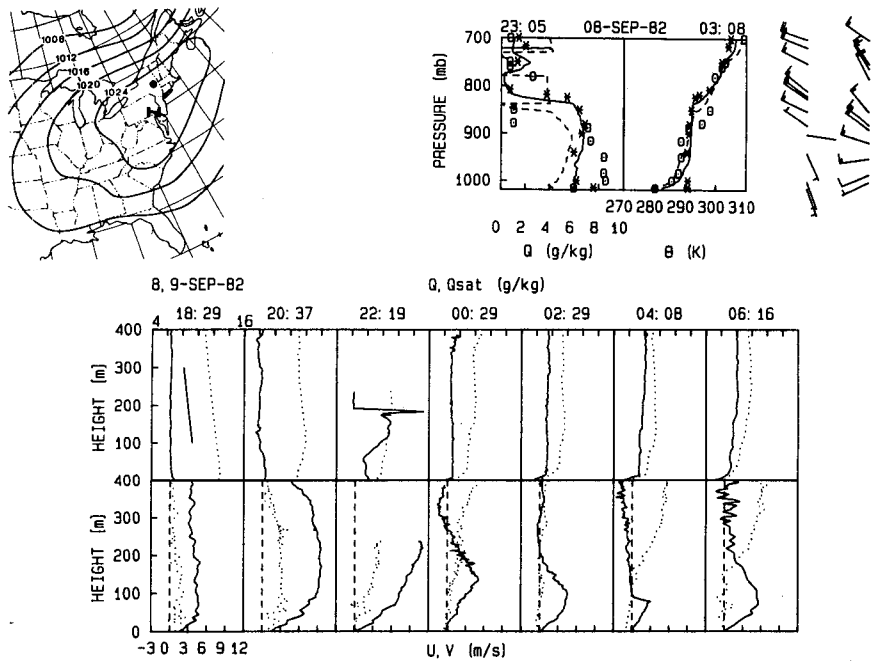

FIG. 8. (a) Observations on 8/9 September 1982. Upper left: Synoptic surface chart at 1200 UTC on 9 September. Upper right: Profiles of specific humidity (Q) and potential temperature (θ) made at Albany airport: Standard radiosonde launches at 0000 UTC (solid line, 2000 local time) and 1200 UTC (dashed line). Additional airsonde launches at times listed at upper left and right of figure are at 2305 (asterix) and 0308 (open circles). At right are wind barbs for the 0000 UTC (left) and 1200 UTC (right) soundings. The series of panels below are profiles obtained with the tethered balloon. Top panel: profiles of saturation specific humidity Q_s (dotted) and Q (solid). The first panel contains a line showing the approximate adiabatic lapse of q_s. Bottom panel: North–south wind component v (solid) and east–west wind component u (dotted).

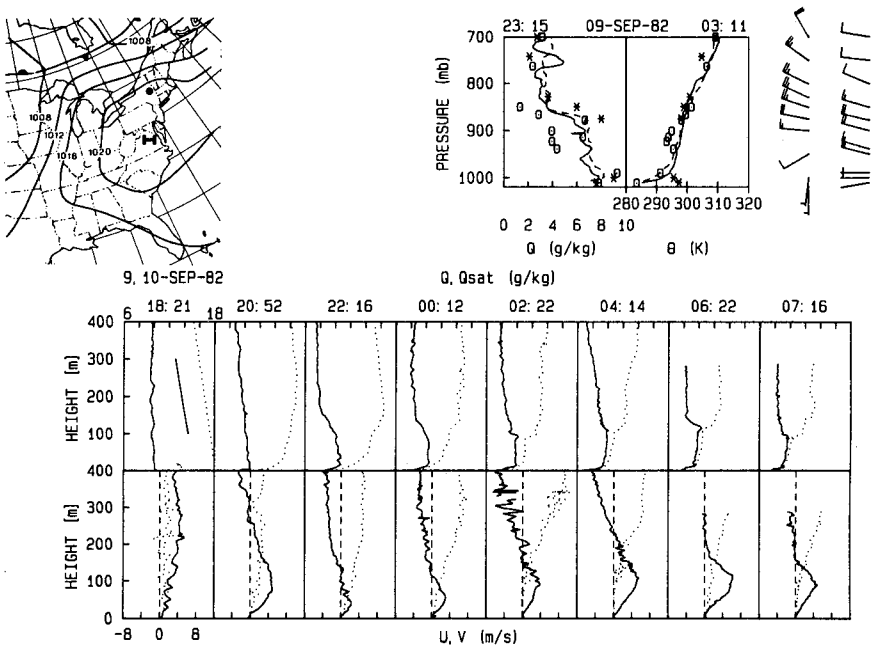

FIG. 8b. Same as (a) on 9/10 September 1982.

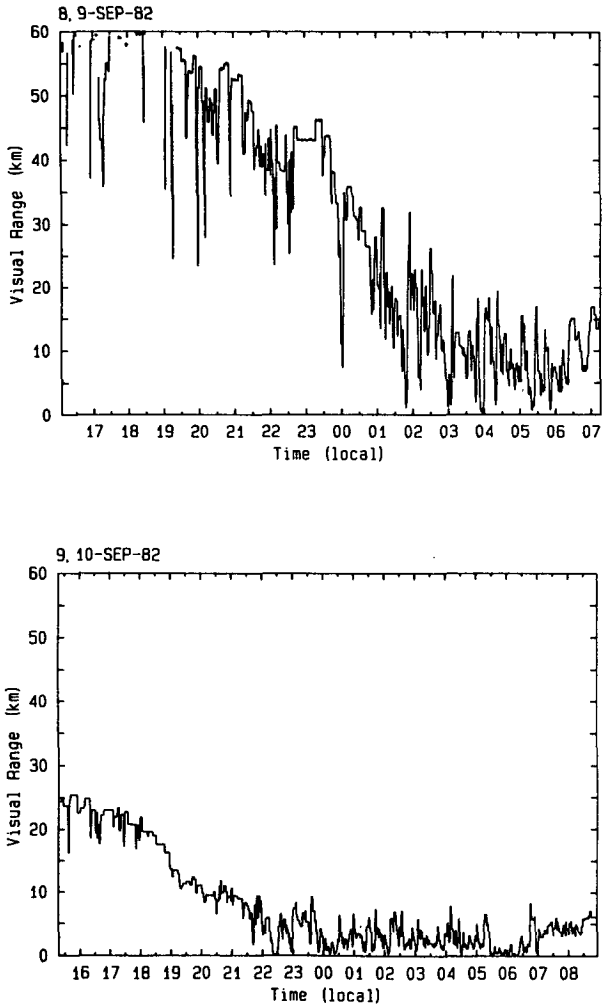

FIG. 8c. Time series of visual range on 8/9 and 9/10 September 1982.

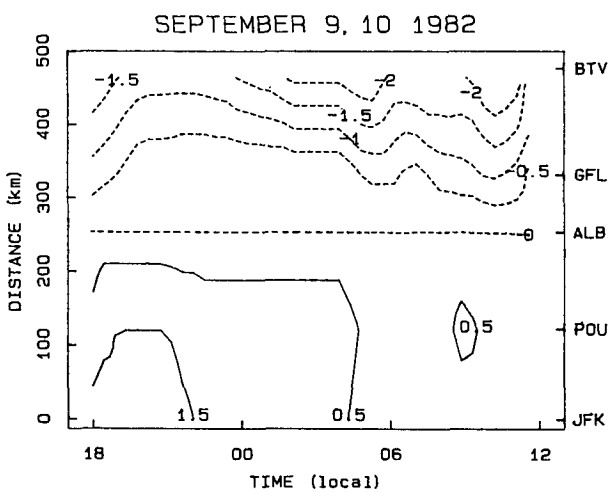

FIG. 8d. Time along-valley distance section of the difference of surface pressure (reduced to sea level) between Albany and other stations (mb). Stations are those identified in Fig. 2.

tethered balloon instrument registered values close to or at saturation, "apparently saturated layers." We do not claim to have measured accurately the humidity very close to saturation with the balloon-borne psychrometer, but it is plausible to say that fog extends through the highest level of apparent saturation.

a. Case 1: 8–10 September 1982 (Fig. 8): Jets along the valley with fog on the second night

The surface high pressure center remained south of Albany during these days. No fog formed on the night of 8/9 September, and the only period of continuous very low visibility occurred between 0530 and 0630 on 10 September. Soundings to 700 mb follow the thermodynamic conceptual model: the afternoon CBL on 8 September reached approximately to 850 mb. Wind in the afternoon convective boundary layer was channeled along the Hudson River valley, in agreement with the conceptual model. The wind direction in the lower half of this layer was upvalley in late afternoon, rotating later from southerly to westerly over the course of the night. A 10 m thick stable surface layer appeared by the 2052 sounding and did not grow appreciably during the night. Strong upvalley flow, at times exceeding 8 m s^{-1}, persisted during most of the night. A sharp region of directional shear is clearly identifiable, even though the level of maximum wind varied during the night. The thermodynamic structure of the remnants of the CBL is evident in all soundings made during the night, but, as the wind rotated, potentially warm, relatively dry air was apparently advected in aloft.

On the night of 8/9 September, a layer from 150 to 300 m deep of wind moved predominantly up the valley. We hypothesize that the low-level wind brought moist air up the valley, but that warm advection was sufficient to avoid saturation (see section 4). The afternoon Albany sounding on 9 September indicates that the moist layer extended only to approximately 910 mb. As on the previous day, rotating winds again led to the drying seen above 950 mb in the morning sounding. There was little mark of the jet in surface measurements. Wind direction frequency roses for the PAM network over the course of the evening show that only some of the surface stations, all located on ridges, were influenced by the jet during the night, though all stations showed along-valley flow during the afternoon. Presence of the jet has many implications for fog formation or pollutant dispersal, but conventional surface wind observations are insufficient to determine its existence. A detailed analysis of observations from the PAM network will appear in a future work.

The synoptic scale surface pressure gradient appears to have been weaker by the morning of 10 September, but the sequence of boundary layer winds on the night of 9/10 September show up-valley motion at 4–5 m s^{-1} up to 150–200 m height, where there was a very shallow directional shear layer. The height of the wind

maximum is lower than that modeled by Gross and Wipperman (1987) for the Rhine valley in Germany. Note formation of a layer approximately well mixed in q and q_s below this shear layer. The jet-like wind profile was persistent, being observed nearly every sounding made between 2100 and 0715. The along-valley surface pressure gradient did not change appreciably during the course of the evening (Fig. 8d), and it is possible that external forcing on the direct channeling was approximately constant during the night.

Specific humidity values below 80 m did not change appreciably over the night of 9/10 September, but the formation of an approximately isothermal layer 70–80 m thick is surprising. Jumps in Θ and q above this shallow layer appear to be associated with westerly advection of dry and potentially warm air. Despite the fact that the early evening boundary layer was drier than on the previous night, the layer to 80 m nearly saturated. Fog occurred (visual range below 100 m) for nearly an hour between 0530 and 0630 10 September. Had the initial condition been slightly more humid, it appears that a fog would have been produced in the nearly saturated layer much earlier. Since this layer was 80 m thick, evidence on other nights indicates the fog could have been persistent.

b. Case 2: 25/26 September 1982 (Fig. 9): Persistent fog with no jet

The high pressure center was northeast of Albany (Fig. 9a), and apparently low-level pressure gradients were not strong. The afternoon CBL reached nearly to 800 mb, with a deep layer moving up the valley. Winds in this layer rotated to easterly during the night, and

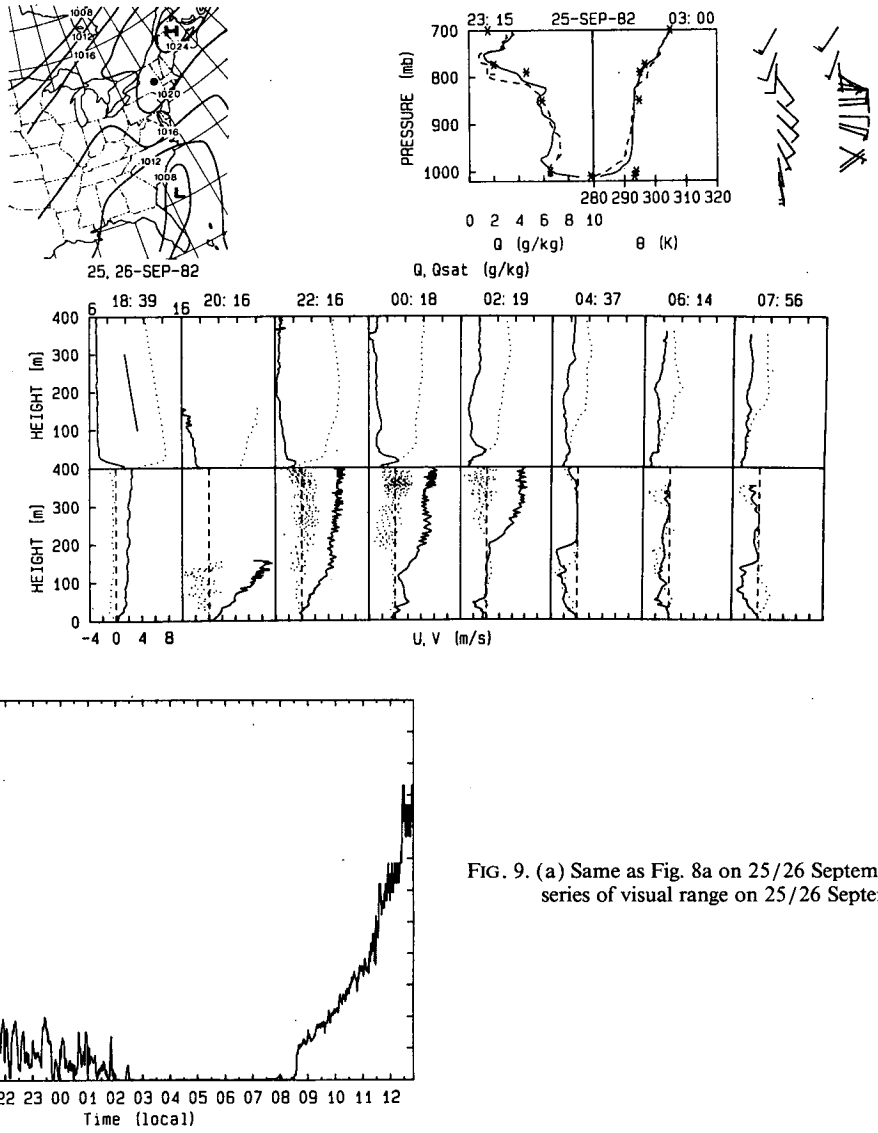

FIG. 9. (a) Same as Fig. 8a on 25/26 September 1982. (b) Time series of visual range on 25/26 September 1982.

boundary-layer values of specific humidity increased slightly during the night.

After a period of strong upvalley winds in the early evening coinciding with enhanced visual range, there was little wind in the boundary layer. A persistent fog occurred from 0200 until 0830 (Fig. 9b). Surface observations indicate that the strong upvalley wind pulse seen in the 2016 tethered balloon sounding lasted less than an hour. The temperature gradient in the surface layer became quite small by 0300. The temperature measured at 0.1 m began to warm at the same time that the visibility began to drop (0200), but that the surface layer took more than an hour to become approximately isothermal. The fog layer thickness did not exceed 20–30 m until after sunrise, when it rose briefly to nearly 100 m thickness. This example illustrates the fog prediction difficulty—even after an entire night of cooling a difference of only a few minutes in the time over which cooling in the boundary layer operates can lead to a total absence of fog, as surface heating begins, or the sudden appearance of a very thick fog layer, as saturation in the boundary layer is finally reached.

c. *Case 3: 30 September–7 October 1982 (Fig. 10): Synoptic high pressure center passes to the south of the Hudson valley*

A high pressure center moved from southwest to south of the site during this period, with a cold front crossing the site by the morning of 7 October. Persistent fogs were seen on the nights beginning with 30 September, 2 October, and 6 October. As the period progressed, nocturnal winds below 400 m were essentially calm (30 September), were mostly northerly (2–4 October), were strong southerly (5 October), and somewhat northerly (6 October). Deep convective boundary layers, nearly to 850 mb, are evident in soundings presented for 30 September, 5 and 6 October. A much shallower (to 900 mb) and somewhat drier CBL occurred on 2 October, as drier, more stable air was advected in from the north. Fog lasted for 5 hours on the morning of 1 October. The apparently saturated layer was 20 m thick at 0034 and had hardly grown thicker by 0423. The next sounding at 0645 shows that there was fog to 120 m. It appears that the layer between 20 and 100 m, cooling largely independently of the surface turbulent exchanges, set the stage for rapid vertical fog growth once the boundary layer wind speed dropped after the 0034. The satellite image made on the morning of 1 October (Fig. 2) shows that fog was extensive in the Hudson, Mohawk, and Connecticut river valleys. The 0749 tethered balloon profile shows that there was little wind in the fog layer, but there was 4 m s^{-1} of westerly shear in the first 100 m layer just above.

Persistent fog was seen on the morning of 3 October only after the northerly boundary layer wind subsided before 0423. The change in direction of the v-component of the wind coincides with a reversal in the north–south pressure gradient observed by standard climate stations all along the valley (Fig. 10f). Note that the surface pressure gradient changed sign at approximately 0200 3 October. The tethered balloon soundings show winds below 200 m moving downvalley at 4 m s^{-1} at least until 0223, were calm at 0423, and then reversed direction, moving upvalley by 0637: Given a more extensive set of boundary layer data, or through careful numerical simulation, it may be possible to relate the occurrence of the jet, its direction and perhaps even its intensity to the observed larger scale surface pressure gradient. The tethered balloon profile sequence on this night shows two layers of approached saturation: a cool layer that grew from 10 to 60 m between 0423 and 0637 and a deeper layer above that reached to 180 m.

On the night of 5/6 October, there was an upvalley wind maximum of 7 m s^{-1} at 150 m. Although the large wind shear surely kept a persistent fog from forming, there is no evidence of a low-level wind maximum in the morning radiosonde data. Wind speeds at 16 m at the base site did not exceed 0.8 m s^{-1} at any time during this night, emphasizing the fact that operational wind data are insufficient information with which to understand the lack of fog on this night. The upvalley jet apparently dropped between the 0420 and 0735 soundings, and a brief period of fog occurred around 0730.

On nights with strong shear, there is sufficient mixing that the surface layer is maintained quite shallow and relatively warm. On these nights, the surface layer is more nearly continuously turbulent. This situation is reflected in estimates of the gradient Richardson number Ri obtained by fitting smoothing splines to the tethered balloon temperature and wind speed profiles. For example, on the night of 5/6 October 1982, Ri at 0020 averaged 0.23, a critical value, in the lowest 30 m, decreasing to values near zero above 50 m where the θ gradient became small, corresponding to the decrease in static stability there. Similar results were found on other nights with jets. That there is continual turbulent mixing can also be inferred by reference to the surface visibility record; strong winds prevented sufficient cooling for persistent condensation in the surface layer.

Winds were lighter on the night of 6/7 October, but the lower atmosphere was much drier at 1800 LST than on the previous night. We observed periods of decreased visibility beginning at approximately 0240 and 0420, but the persistent fog period began only at 0540. The apparently saturated layer at that time reached only to 30 m. At 0520 on this night, during the single hour-long period of persistent fog, the visual range was observed to fall below the fog threshold at 10 m altitude nearly 15 minutes *before* it did at 1.5 m. This is the only example presented in this paper of the

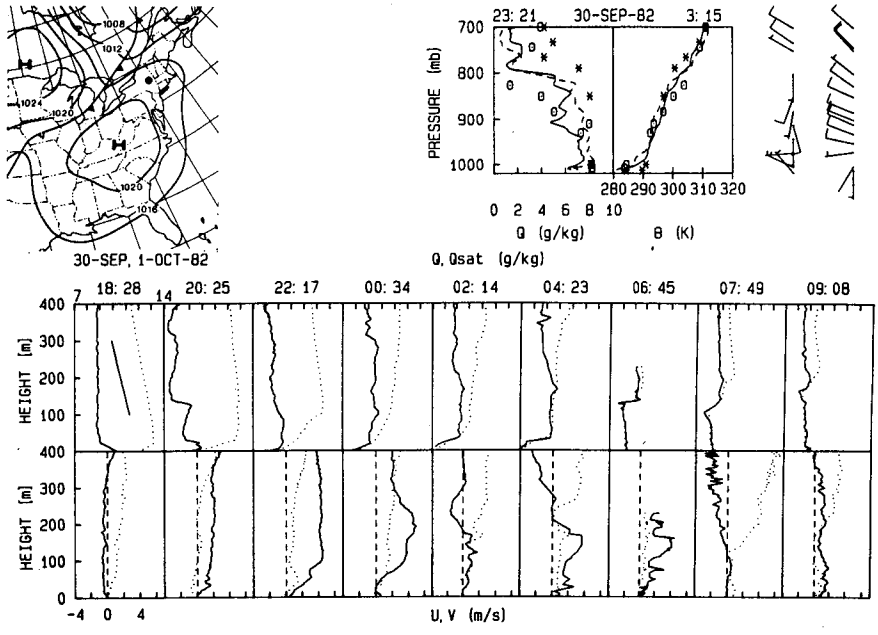

FIG. 10a. Same as Fig. 8a on 30 September–1 October 1982.

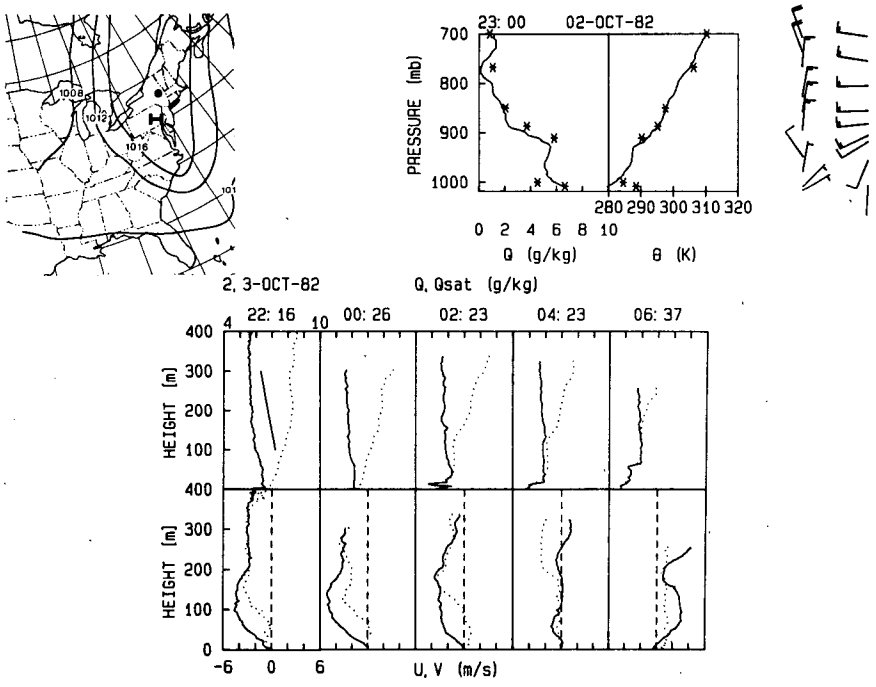

FIG. 10b. Same as Fig. 8a on 2/3 October 1982.

fog forming first at the upper level, though this is not the only occurrence that has been observed. Since a northerly jet is seen on this night (Fig. 10d), this sequence in visual range was possibly the result of advection of a fog that initially formed over the Mohawk River, though confirmation of this hypothesis awaits further field observations.

d. Case 4: 10/11 October 1982 (Fig. 11): Deep fog evolution as the along-valley wind reverses

The high pressure center was to the north of the site. A moist CBL extended to just below the 900 mb level on the evening of 10 October. Radiosonde winds show that the wind rotated toward southerly during the night.

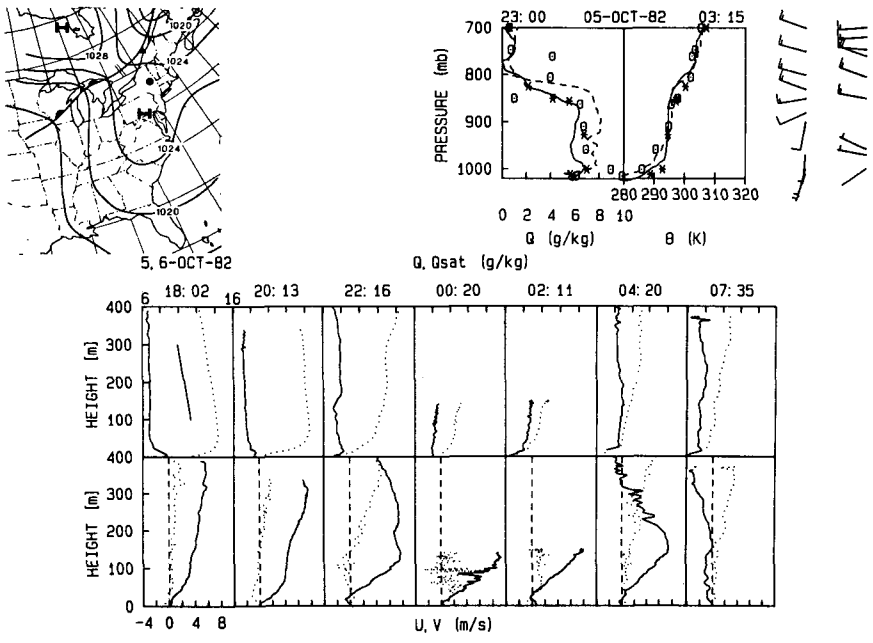

FIG. 10c. Same as Fig. 8a on 5/6 October 1982.

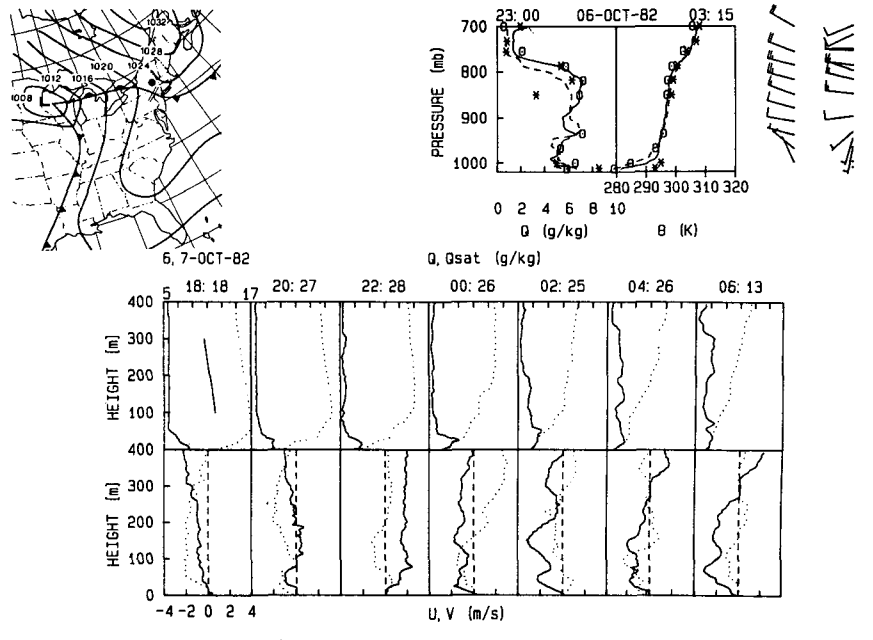

FIG. 10d. Same as Fig. 8a on 6/7 October 1982.

Tethered balloon profiles show initial moist conditions in the lowest 400 m at 2031. Persistent fog began at 0200 and lasted until 0900 with periods of relative clearing between 0500 and 0700, with the visual range dropping below the fog threshold at the 10 m level approximately 5 minutes before it did so at the 1.5 m level. During the first foggy period, the surface layer remained stable even as the visibility was reduced to near zero, indicating that the early evening fog was shallow. The fog layer grew in thickness over the early morning hours, from 10 m at 0015, 30 m at 0444, dropped to 30 m in the sounding made during clearing at 0621, but was at 80 m and 190 m for the 0825 and 0938 soundings respectively. The surface heat budget indicates that the surface layer changed from stable to nearly neutral after fog formed during the first period.

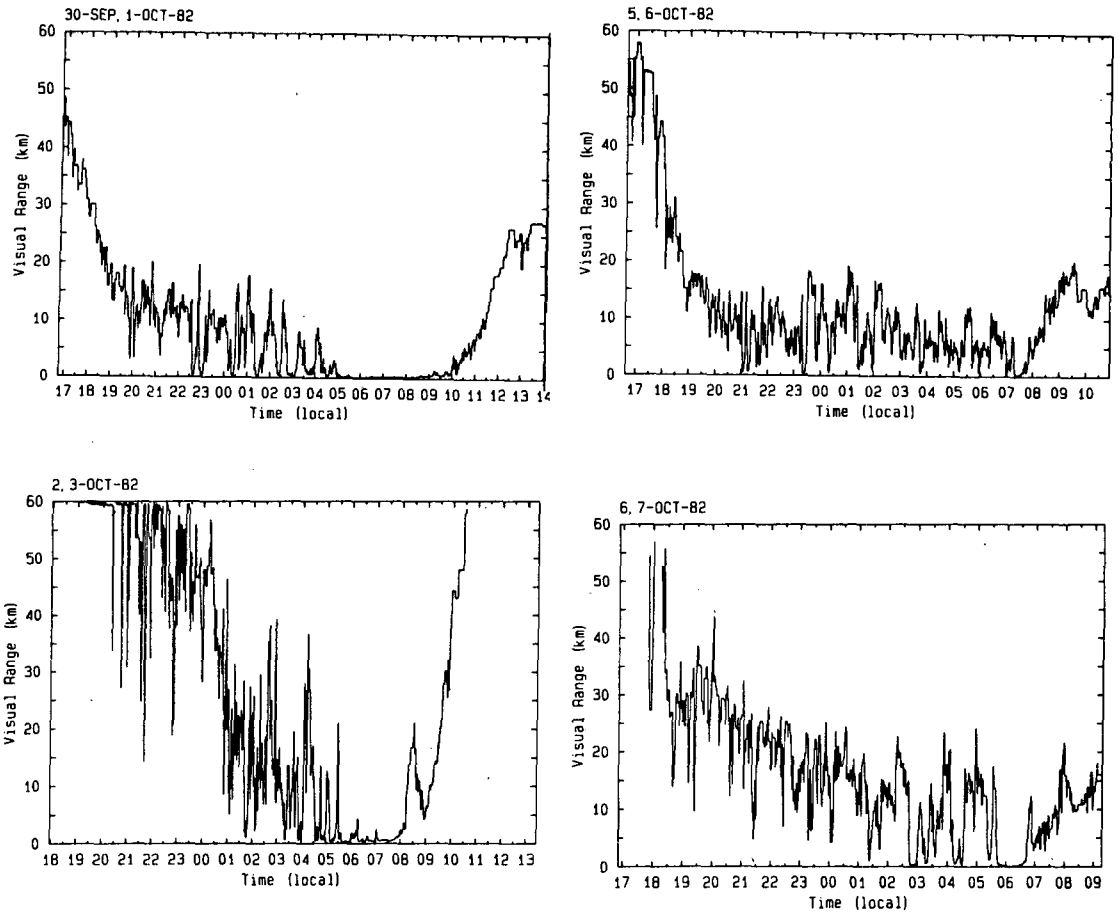

FIG. 10e. Time series of visual range on 30 September/1 October 1982, 2/3 October 1982, 5/6 October 1982, and 6/7 October 1982.

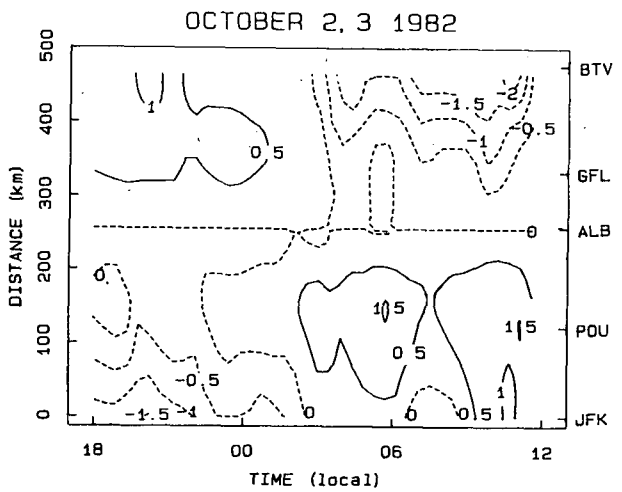

FIG. 10f. Time–along-valley distance section of the difference of surface pressure (reduced to sea level) between Albany and other stations (mb) on 2/3 October 1982. Stations are those identified in Fig. 2.

During the second period of reduced visibility, beginning after sunrise at approximately 0700, the surface layer was convective, and the fog layer grew rapidly to 100 m thickness by 0756. An inversion in q_s (and hence θ) developed above a nearly saturated layer. Surface visibility began to improve at approximately 0900, though the sounding at 0938 shows that there was still a deep, saturated layer. Winds were light within the fog, with sharp westerly shear in the layer above leading to 6 m s^{-1} winds at 250 m. This is clear illustration of how a developed, thick fog can modify the wind profile, forcing shear to concentrate at the fog top inversion. Since the visibility had already begun to increase by 0938, we surmise that the fog cleared from below.

e. Case 5: 12–14 October 1981 (Fig. 12): Northerly jet with synoptic high pressure center passing to the north of the Hudson valley

On 13 October, the surface chart shows that Albany was near the center of a high pressure cell that elongated

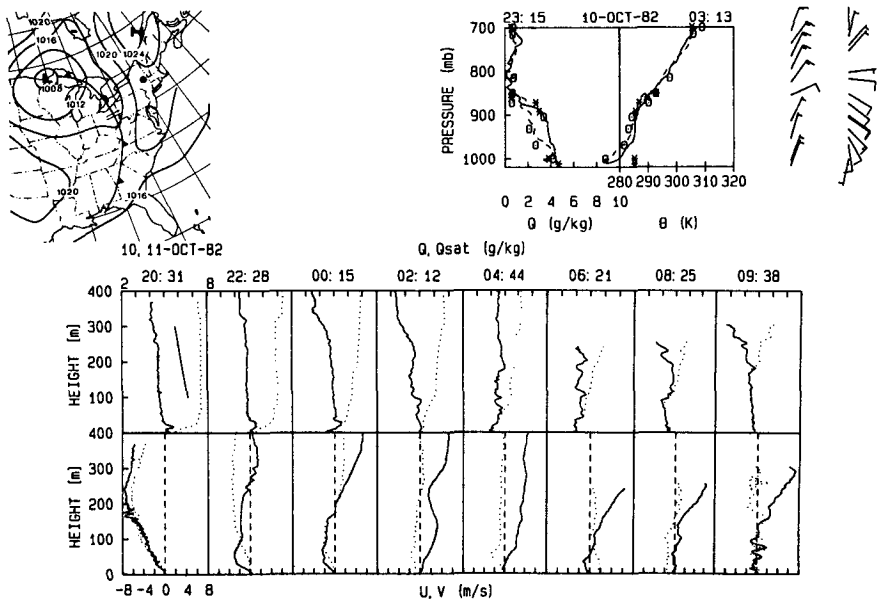

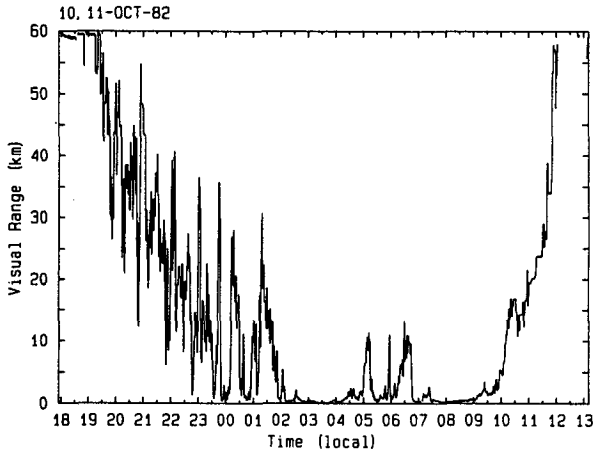

FIG. 11. (a) Same as Fig. 8a on 10/11 October 1982. (b) Time series of visual range on 10/11 October 1982.

and moved east the following day. Radiosonde and airsonde profiles over the night of 12/13 October give evidence of a moist layer remnant CBL to approximately 900 mb, capped by a stable inversion layer. Winds through this layer were northerly at all levels during the night. Despite the presence of large shear in the lowest 80 meters, persistent fog formed just before 0430 and lasted until 0820. Humidity profiles indicate that the apparently saturated layer reached to approximately 80 m by 0625. The surface layer was quite stable until 0600; fog formed before sunrise, at 0430. Maximum fog thickness did not exceed 20 m before sunrise or 50 m thereafter.

On the following day, the CBL and the moist layer were much shallower. By morning on 14 October, the low-level wind shifted to southerly. Only patchy fog was observed on this night, though winds were much lighter than on the previous night. Above 30 m height, the boundary layer was somewhat drier and warmer than on the preceding night. Boundary layer profiles show a saturated layer only to approximately 40 m by 0612. The environment was too warm and stable to support a persistent fog except for the brief period between 0630 and 0700.

f. Case 6: 27–29 October 1982 (Fig. 13): Moist layers between 20 and 100 m determined by shifts in wind direction

Visual range dropped below 10 km on each of these nights, but no fog formed. The surface high pressure center moved from the southwest of the site toward the south during this period. Boundary layer winds were substantially higher on the night of 28/29 October than they were on the preceding night. The soundings to 700 mb show that there was a moist layer to ap-

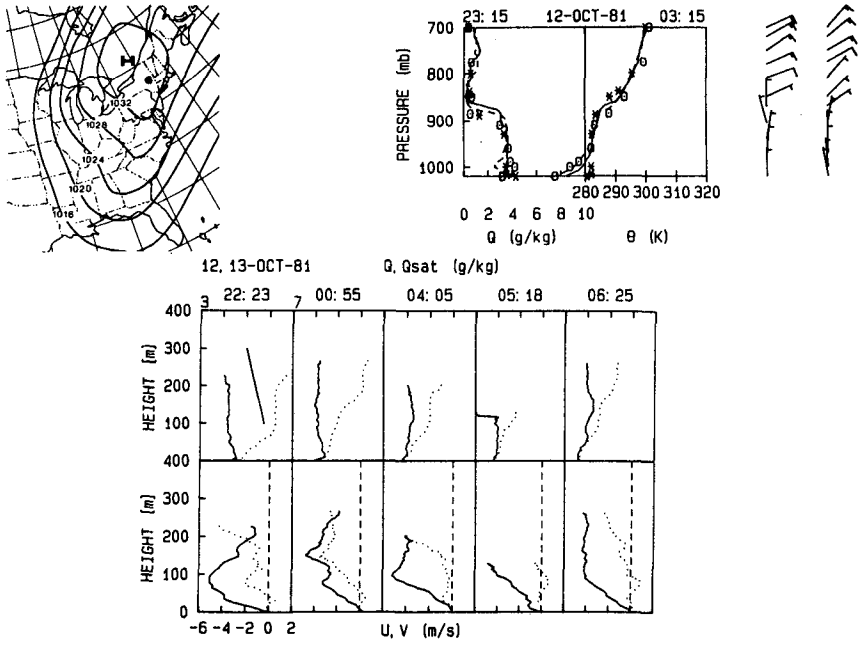

FIG. 12a. Same as Fig. 8a on 12/13 October 1981.

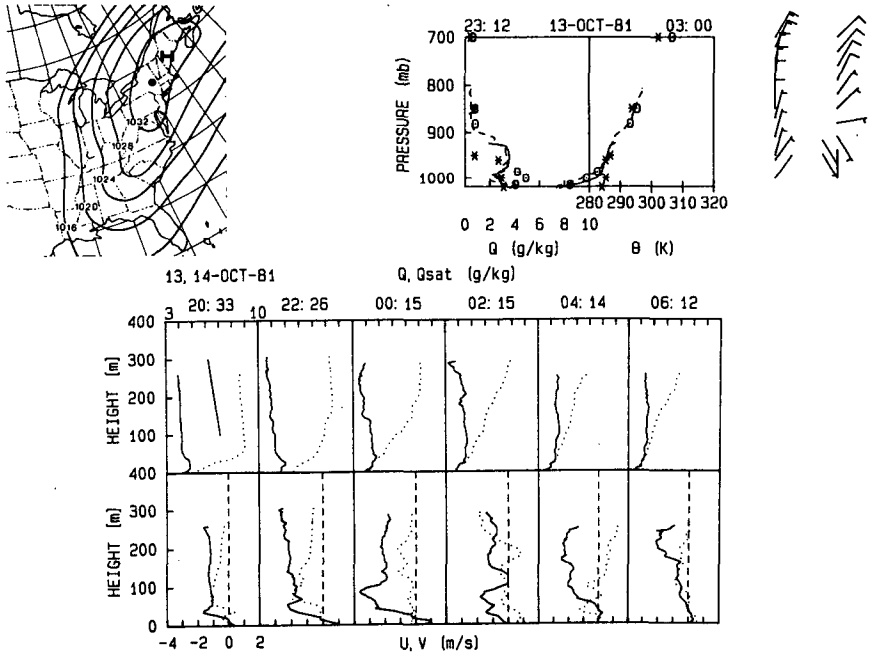

FIG. 12b. Same as Fig. 8a on 13/14 October 1981.

proximately 920 mb, with another moist layer above 800 mb. Winds are quite weak to 700 mb. A low-level upvalley wind maximum that quite similar to that seen on 5/6 October, appeared by 2013 and persisted until 0626. At approximately the level of this wind maximum, a jump in q_s is evident by 2209 and this discontinuity sharpens over the evening. There is no evidence for this nocturnal upvalley flow in the morning operational sounding. Winds at 16 m at the base site do not exceed 1 m s^{-1} during the entire evening. A striking feature of the tethered balloon soundings on 28/29 October is the evolution of q and q_s profiles nearly constant with height up to ~125 m, even though this layer apparently is never saturated above 20 m. Reference

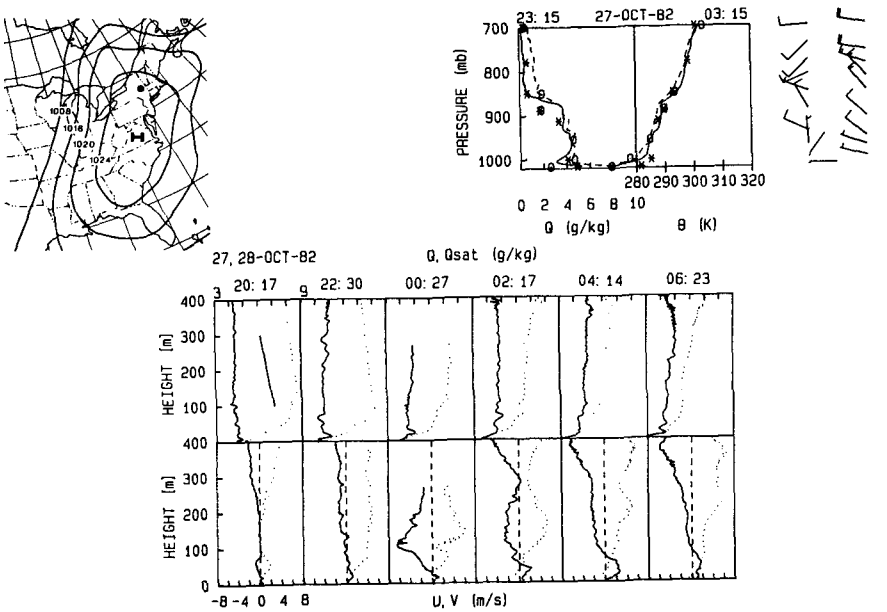

FIG. 13a. Same as Fig. 8a on 27/28 October 1982.

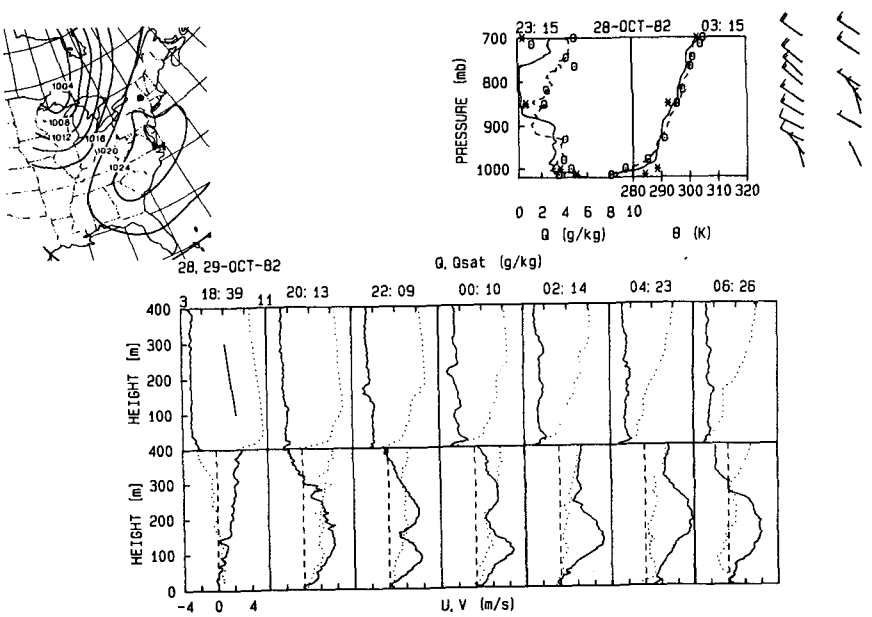

FIG. 13b. Same as Fig. 8a on 28/29 October 1982.

to the wind profiles shows that this inversion coincides approximately with the level of maximum wind in the southerly jet that persisted that night.

What is clear from this case is that the saturation deficit in the boundary layer below 100 m altitude varies rapidly as the along-valley wind direction changes from northerly to southerly, effectively changing τ_f with each reversal. We emphasize that, at Albany, fogs that have long periods with persistently low visual range are thick, boundary layer fogs, and that the boundary layer fog environment appears to be strongly modulated by moisture advection brought about by the vicissitudes of local winds.

g. *Estimating the saturation deficit budget*

The cases just presented lead to estimates of the terms in the boundary layer humidity deficit budget. The approach here is to make estimates of the magnitude of some of the terms in the saturation deficit budget equations (1) and (2). Those terms in those equations are 1) local change, 2) radiative cooling, 3)

turbulent flux divergence, 4) horizontal advection, 5) drying or warming effects of large-scale subsidence. Estimates of 1) are made using the time series of tethered balloon soundings and of 2) using the radiative transfer model incorporating observed T and q profiles. We make rough estimates of horizontal advection 4) using surface station data along the valley with winds from the tethered balloon profiles. Although estimates of subsidence based on radiosonde profile sequences were done in Carlson and Stull (1985), we note that mean gradients in the remnant convective boundary layer are small and ignore this term in the current work, following the scaling arguments presented in Garratt and Brost (1981). It seems much more likely that horizontal, not vertical advection is more important to the Albany fogs. Since our direct measurements are only of mean quantities, we can offer only some hypotheses concerning the vertical extent of the importance of turbulent transport based on the residual of the radiative flux divergence and the local change term.

1) Local change and radiative cooling

The average local change $\partial T/\partial t$ was obtained over the night by differencing temperature profiles observed in the boundary layer closest either to fog formation or to dawn with the profile obtained early in the evening (at 1800 or 2200, as available). The difference profiles were obtained by interpolating the raw tethered balloon descent profiles to fixed levels using a smoothing spline. For the most part, the total cooling rate profiles approach nearly constant values ranging from 0.2 to 0.5 K h^{-1} above 250 m altitude for our cases. Total cooling rates exceeding 1 K h^{-1} were never observed. Four example profiles are shown in Fig. 14. Even though the low-level jet was present on the nights of 9 September and 27 October, the total cooling rate is larger than on the two nights, 30 September and 10 October, when no high boundary layer winds were observed.

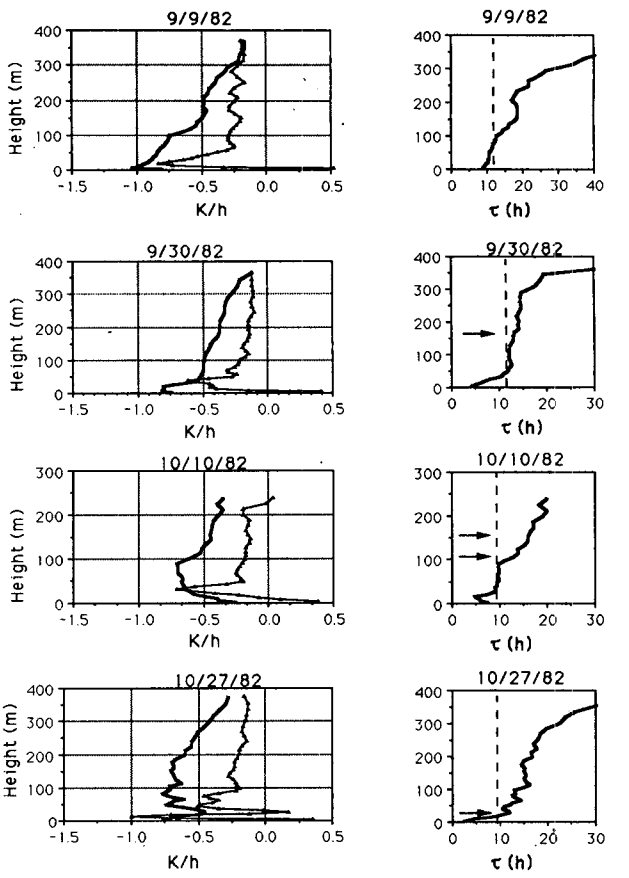

FIG. 14. Left column: Profiles of total cooling rate $\partial T/\partial t$ (heavy solid line) and radiative cooling rate based on the earliest tethered balloon sounding (thin solid with triangles) on the evenings of 9 and 30 September, and 10 and 27 October 1982. Right column: Estimates of the time required for the boundary layer to reach saturation (τ) found using the earliest sounding and the observed total cooling rate corresponding to the same evenings. Arrows mark the height to which deep fogs were observed to form. Two arrows on "10/10/82" correspond to the fog thickness before (lower arrow) and after (upper arrow) sunrise.

Estimates of the radiative cooling rates from the Roach model for two examples are also presented in Fig. 14. A puzzling result is that, although profiles of $\partial q/\partial t$ typically indicate an absence of turbulent moisture exchange above the lower 20 m, as in Fig. 6a, radiative cooling alone cannot account for the total cooling rate above this level. We have investigated the sensitivity of the radiative cooling model and found it impossible to get significantly higher clear-air cooling rates using observationally consistent temperature and humidity profiles. One sees limited variability in radiative cooling rates for the four cases in Fig. 14. There is in these and other cases an "unexplained" cooling rate of 0.2 to 0.3 K h^{-1}. Along-valley horizontal advection, if it were important at all, would have contributed to *warming* on many of these nights. We can find no plausible reason for which to doubt the temperature observations and accordingly offer two alternate hypotheses for the discrepancy between total and radiative cooling rates: 1) The difference may be ascribed to turbulent flux divergence through a layer 300 m thick, as Stull (1988) suggests when offering other examples with similar features and 2) cross-valley cool advection caused by converging katabatic winds that overrun the colder surface layer led to the cooling. Maki and Harimaya (1988) observed that accumulation of cool air in valleys and basins leads to larger cooling rates in such regions in comparison to flat areas. That the total cooling rate appears to approach the calculated radiative cooling rate in the layer above 300 m height (Fig. 14), approximately the altitude of the valley sidewalls, lends credence to this hypothesis. Preliminary numerical simulation of pooling of cool air despite moderate cross-valley flow in a valley with geometry

similar to that of the Hudson valley (P. K. Smolarkiewicz, personal communication) also indicates that the cool pool is comparable to the valley side wall height. Our data are not complete enough to distinguish these alternatives, but it appears that 2) is more plausible. To accept 1), we must assume that the measured surface fluxes (Table 2), too low by far to converge to provide the missing cooling, simply do not represent the valley at large. Testing these hypotheses is an appropriate use of a mesoscale model simulation; work in this direction is already in progress.

We calculated the profile of τ_f a posteriori using the observed cooling rate profile along with the relative humidity profile obtained at dusk. Since we use observed cooling rates, this procedure obviously does not constitute a prediction technique. The time to reach saturation, τ_f, increased abruptly above 100 m altitude on 9 September (Fig. 14) both because $\partial T/\partial t$ decreased with height and because the initial relative humidity was higher there. The τ_f profile for the 30 September case illustrates that the fog grew in a fertile environment, and that it would have grown much deeper had the night been longer. The case of 10 October is particularly interesting. The level to which fog grew up until dawn (the lower arrow in the τ_f profile in Fig. 14) agrees well with what one would expect given the initial conditions. The second arrow indicates the height to which fog grew after sunrise, and this level was poorly predicted by this method. Reference to Fig. 11a indicates that the layer above 100 m was becoming more moist over the course of the morning hours.

In Table 4, the observed total cooling rate was also used to estimate average τ_f in the lowest 50 m for all of our cases. Using τ_f to predict likely fog nights is only partially successful. Of the 14 cases with 7 persistent and 3 patchy fogs presented here, an arbitrary rule predicting fog when $\tau_f < 10$ hours is successful for two cases without fog, fails on two of three nights with patchy fog, and predicts seven of eight occurrences of persistent fog. On the night of 6/7 October 1982, τ_f was large (11 h) and the rule fails, but the persistent fog that formed was quite shallow, never reaching above approximately 30 m. There is also some evidence that shallow, persistent fogs at the Albany airport site may reflect the influence of the nearby Mohawk River, though testing this hypothesis awaits further field study.

The implication for forecasting in the early evening is that a model or empirical prediction of the cooling rate above the surface layer can be substituted for $\partial T/\partial t$ in (1) to give a first estimate of the time required to fog the boundary layer under clear-sky conditions. If the range of variation in total cooling rate profile can be established through modeling or empirical methods, we can use τ_f to predict fog likelihood. Although the range of average total cooling rates in the 0–50 m layer (Table 4) varies from −0.6 to −0.9 K h^{-1}, τ_f varies over a larger range, from 4 to 15 hours.

2) HORIZONTAL ADVECTION AND LOW-LEVEL JETS

The primary source of cooling is radiative, but the other factors may be important in deciding whether or not a likely fog environment leads to a persistent fog. On many occasions, we have seen layers with strong along-valley flow, following essentially the pattern given in the local wind conceptual model of section 2. Thus, advection could be important given sufficient horizontal temperature gradients. We think that this jetlike structure, not noted previously as characteristic flow in the Hudson valley, may be important not only to fog prediction, but also to forecasting nocturnal pollutant transport. Unfortunately, we have the least information about this term.

In many cases, winds to 900 mb were oriented along the valley axis during the afternoon, and rotated toward the direction of the 850 mb flow early in the evening. The wind rotation occurred at least down to 400 m height. When the 850 mb wind did not change appreciably over the night, the wind at 400 m rotated approximately to the geostrophic direction within two

TABLE 4. Summary of boundary layer properties.

Date	Fog (F) Patches (P) No fog (O)	Jet along-valley ± (altitude)	CBL top (mb)	$\bar{q}_{CBL}$ (q kg^{-1})	Surface pressure $P_{POU} - P_{ALB}$ (mb)		$Z < 50$ m $\mathbf{V} \cdot \nabla\theta$ (K h^{-1})	$Z < 50$ m $\partial T/\partial t$ (K h^{-1})	τ_f(h) $Z < 50$ m
8/9 Sep	0	+100 m	850	6	1.4	0.9	0.5	−0.7	15
9/10 Sep	P	+100 m	900	8	1.2	0.8	0.1	−0.9	10
25/26 Sep	F	—	830	6	0.2	−0.1	−0.2	−0.9	8
30 Sep/1 Oct	F	—	840	7	0.4	0.6	0.1	−0.8	8
2/3 Oct	F	—	920	5	0.2	0.4	~0	−0.6	4
5/6 Oct	P	+120 m	860	6	−0.1	−0.3	0.4	−0.7	13
6/7 Oct	F	—	800	6	−0.1	−0.3	−0.2	−1.0	11
10/11 Oct	F	—	900	4	+0.4	+0.6	~0	−0.6	6
12/13 Oct 1981	F	−80 m	880	3	—	—	—	−0.6	6
13/14 Oct 1981	F	—	980	4	—	—	—	−0.8	7
27/28 Oct	P	—	900	4	+0.3	+0.7	~0	−0.7	8
28/29 Oct	O	+100 m	950	3	+0.6	+0.8	−0.1	−0.8	14

hours of sunset and did not change thereafter, not behavior characteristic of an inertial oscillation. For example, on the night of 9/10 September 1982 (Fig. 8), the wind direction remained slightly north of west above 900 mb, the apparent afternoon CBL top. The wind at 400 m rotated from southerly to this direction in at most two hours, twice as fast as one expects from an inertial oscillation at this latitude. We hypothesize that this rapid turning toward the geostrophic direction occurs during the transition period, when the surface layer decouples from the convective boundary layer but decaying convective eddies continue dynamical coupling of the top of the mixed layer to the free atmosphere above. In no case did we see a wind maximum above 100 m; wind maxima in the nocturnal boundary layer were always aligned approximately north and south, along the valley axis.

Profiles made at a single station are insufficient to allow us to conclude that along-valley wind maxima below 100 m height are extensive. We have found, however, that the presence and direction of this wind can be predicted knowing the surface pressure gradient reported by stations along the Hudson river valley. The 9/10 September 1982 and 2/3 October 1982 cases presented above illustrate our point. The time sections of the difference of sea-level pressure between Albany and stations along the valley (Figs. 8e and 10g) lead us to expect that the jet-like feature only appears when there is a sufficient along-valley pressure gradient. A summary of the surface pressure difference between Poughkeepsie and Albany on all case study nights (Table 4) shows that we did not observe the low-level wind maximum unless the surface pressure gradient exceeded 1 mb over this distance ($\sim$100 km). Even though these pressure differences are quite small, these results indicate that it may be possible operationally to use this information to predict the existence of the low-level wind maxima. Currently, there is no routine way to obtain winds at 50–200 m altitude with sufficient accuracy to observe the jet.

While one might explain the observed afternoon along-valley winds by reference to frictional inflow, enhanced by the difference in roughness between the valley floor and the surrounding higher ground, it seems much less plausible during the night. There must be some cross-valley pressure gradient to balance the Coriolis force, and it seems reasonable to associate this pressure gradient with a cross-valley slope in the cool layer usually found below 100 m in the soundings. Future observations and model simulations are planned to study the continuity of the wind maximum along the valley and the presence of the cross-valley pressure gradient.

We made a crude estimate of the advection term in the along-valley direction, calculating $-v_h \partial\theta/\partial y$ using the difference in potential temperature (to account for differences in station altitudes) reported by the standard surface meteorological stations at Poughkeepsie and Albany, replacing v_h with the *maximum* v-component of the wind seen in the boundary layer, usually below 200 m. We are assuming essentially that the vertical θ profiles are similar at each station. Estimates were made for each tethered balloon sounding, then averaged over the course of the evening. The two largest estimates of advective warming occurred on 8/9 September (+0.5 K h^{-1}) and 5/6 October (+0.4 K h^{-1}), both high-wind nights with patchy or no fog at the base site. Turbulent mixing in the lowest 200 m on these nights could only warm the surface layer. It could not lead to appreciable drying because there was little vertical q gradient. That the boundary layer did not saturate was probably due, at least in part, to the delaying effect of warm advection, though strong turbulent mixing diluted cooling effects seen at the surface through a deeper layer. In each case, the entire layer below 400 m approached saturation, but did not quite make it. Warm advection on these nights may have been sufficient to prevent fog formation. Though these estimates of advective warming are quite crude, they point the way for planning subsequent observational and modelling studies.

6. Conclusions and suggestions for further work

Through analysis of a number of occurrences of fog in the Hudson valley, we have identified a number of conditions that promote fog, and these can be considered collectively to represent fog environments. To describe the environments we are obliged to consider mechanisms of turbulent exchange in the surface layer and the controls on heat and moisture advection produced by nocturnal boundary layer flows.

1) The end of the period of decay of mechanical turbulence in the surface layer during the early evening transition can be associated with a change in the sign of the temporal curvature of the mean temperature, $\partial^2 T/\partial t^2$.

2) Turbulent moisture flux convergence into the surface layer during the early evening transition leads to a jump in specific humidity from 1 to 3 g kg^{-1}. This jump appears to be a commonplace phenomenon. It reduced the expected time for the surface layer to reach saturation by several hours for many of the fog cases. One can estimate the time at which this may occur by identifying the inflection point in the mean surface temperature trace, using 1).

3) Most cases showed that the evening began with a deep moist layer (the afternoon CBL) that extended to from 920 to 850 mb, generally following the conceptual model presented in section 2. Winds in the remnant CBL rotated toward the 850 mb wind direction (and presumably close to geostrophic) during the night. No jet that one might associate with the inertial oscillation (Blackadar 1957) was seen in this layer.

4) Periods with visual range less than 100 m did not occur near the ground until the surface layer reached apparent saturation (e.g., Fig. 3a). When the tethered balloon profiles indicated that there was such a layer no thicker than 20 m, we always observed much variation in the surface visibility, and observers reported patchy fog (e.g., Fig. 9b, from 2200 to 0200 LST). Higher winds associated with increased visibility on nights when the nearly saturated layer was quite shallow but did not prevent deep fog formation when the boundary layer was initially close to saturation (e.g., the 9/10 September case, Fig. 8c). During nights with persistent fogs (periods longer than 30 minutes' duration of low visual range at the surface) occurred only when fog layers were at least thicker than 50 m (e.g., the 25/26 September case, Figs. 9a and 9b).

5) Whether or not fogs formed, little change in the specific humidity was observed in the layer from 20 to 100 m during the night. Changes in humidity above this level were associated with wind direction shifts, and are probably associated with dry advection. Below this level, specific humidity was close to saturation, dropping with the temperature. Fogs in this layer apparently do not form primarily because of increasing specific humidity, but rather simply because of cooling. The cooling may be due to radiative heat loss, possibly modified by advection. If the layer between 20 and 100 m saturates quickly enough, thick and persistent fogs form.

6) Regular evolution in the stable boundary-layer structure is reasonably well described by 2-hourly tethered balloon profiles. This regularity is particularly striking when one considers that we present the unsmoothed, raw tethered balloon descent profiles in this work. Nocturnal winds in the lowest 100 m blow parallel to the Hudson valley axis, and on many nights winds with maxima from 4 to 7 m s^{-1} below the 100 m level occur. These winds would not be noted if one referred only to standard surface and radiosonde data. Time–valley sections of surface pressure (Figs. 8e and 10g) lead us to suggest that presence of the low-level jet structure may eventually be associated quantitatively with a critical value of the along-valley pressure gradient. On several cases with jetlike winds, the layer up to the wind maximum appears to be well mixed in q and q_s, profiles that resembling those of mature deep fog even *before* the layer saturated.

7) Satellite images demonstrate that many of the thick, persistent fogs we saw at Albany were widespread, extending throughout the Hudson and Connecticut river valleys. This indicates that initial conditions seen on these nights at Albany can be widespread. The heat balance in the boundary layer indicates that the fog is confined to the valley both because moisture may be initially higher there and can be maintained higher by predominantly along-valley winds and possibly because drainage flows from the valley wall leads to cold pooling. We hypothesize that cold pooling of katabatic winds from the valley sidewall may flow above the surface layer, but this hypothesis is tentative and awaits further tests.

8) Because of the importance of processes occurring in the layer from 50 to 200 m to persistent fog development, it is clear that prediction schemes that rely only on local operational data, which provides little data about conditions in the layer from 10 to 500 m altitude, can be quite limited. Fog prediction schemes must infer conditions 20–40 m above the surface in a systematic way. One possible technique is the following: extrapolate surface observations made at approximately the heat flux crossover time upward adiabatically to give the q_s profile and take the q profile to be constant at its value at that time. Then use historical or model-derived cooling rates to estimate τ_f, the time required for the boundary layer to reach saturation.

Fogs in the Hudson valley occur when the environment supports them, but determination of the supportive environment involves more than the traditionally considered surface layer observations. Deep fogs at Albany and along the valley are boundary layer phenomena, and they occur when boundary layer circulations are either weak or are such that sufficient moisture is maintained above the surface layer. To the first approximation, the surface layer appears to be largely decoupled from the boundary layer on many fog nights, and the presence of decreased visibility below 20 m offers little information about the likelihood of deepening fogs later. In many cases, the ultimate depth to which the fog grows may be determined by dry advection resulting from the boundary layer wind rotation. One must therefore take special care, therefore, when "verifying" simple one-dimensional models with field observations to take into account what is occurring in the boundary layer prior to fog formation.

Both numerical and further observational studies should be done to test our inferences. In particular, a mesoscale numerical simulation of a case like 9/10 September 1982 would be of great value in determining likely locations for fog location on nights that exhibit the jet. Subsequent observational studies should aim also toward identifying the spatial continuity of the jet. Further detailed model studies using the 30 September and 11 October 1982 cases as prototypes could examine the extent to which fogs modify their own environment and the role of entrainment in fog growth. We suggest that a better understanding of the boundary layer dynamics, coupled with relatively simple parameterizations of radiative cooling and cloud microphysics, may offer the most fruitful approach to the radiation fog prediction problem.

Acknowledgments. This work was supported by National Science Foundation Grant ATM8317455 and United States Army Research Office Grant

DAAG2984K0050. We appreciate the diligence of L. Dzamba, who aided in the data analysis. Management of the FOG-82 dataset was made much easier because of the programming efforts of M. Meyer and the technical support of J. Sicker. The efforts of the field personnel who cooperated during the FOG-82 observation program are also gratefully acknowledged.

REFERENCES

Ackerman, S. A., C. Johnson-Pasqua and S. K. Cox, 1982: Surface radiation budget during FOG Project-1982 in Albany, New York, Fog-82: A Cooperative Field Study of Radiation Fog. ASRC-SUNY Publ. No. 984. [Available from Atmospheric Sciences Research Center, 100 Fuller Road, Albany, NY 12205.]

Aitken, J., 1885: On dew. *Trans. R.S.E.*, **33,** 134–186.

Blackadar, A. K., 1957: Boundary layer wind maxima and their significance for the growth of nocturnal inversions. *Bull. Amer. Meteor. Soc.*, **38,** 283–290.

Brost, R. A., and J. C. Wyngaard, 1978: A model study of the stably stratified planetary boundary layer. *J. Atmos. Sci.*, **35,** 1427–1440.

Businger, J. A., J. C. Wyngaard, Y. Izumi and E. F. Bradley, 1971: Flux profile relationships in the atmospheric surface layer. *J. Atmos. Sci.*, **28,** 181–189.

Carlson, M. A., and R. B. Stull, 1985: Subsidence in the nocturnal boundary layer. *J. Climate Appl. Meteor.*, **25,** 1088–1099.

Caughey, S. J., and M. Kitchen, 1984: Simultaneous measurements of the turbulent and microphysical structure of nocturnal stratocumulus cloud. *Quart. J. Roy. Meteor. Soc.*, **110,** 13–34.

——, W. M. Dare and B. A. Crease, 1978: Acoustic sounding of radiation fog. *Meteor. Mag.*, **107,** 103–113.

——, J. Wyngaard and J. C. Kaimal, 1979: Turbulence in the evolving stable boundary layer. *J. Atmos. Sci.*, **36,** 1041–1052.

——, B. A. Crease and W. T. Roach, 1982: A field study of nocturnal stratocumulus: Part II–Turbulence structure and entrainment. *Quart. J. Roy. Meteor. Soc.*, **108,** 125–144.

Findlater, J., 1985: Field investigations of radiation fog formation at outstations. *Meteor. Mag.*, **114,** 187–201.

Fleagle, R. G., W. H. Parrott and M. L. Barad, 1952: Theory and effects of vertical temperature distribution in turbid air. *J. Meteor.*, **9,** 53–60.

Funk, J. P., 1960: Measured radiative flux divergence near the ground at night. *Quart. J. Roy. Meteor. Soc.*, **86,** 382–389.

Garratt, J. R., and R. A. Brost, 1981: Radiative cooling effects within and above the nocturnal boundary layer. *J. Atmos. Sci.*, **38,** 2730–2746.

Gross, G., and F. Wipperman, 1987: Channeling and countercurrent in the upper Rhine valley: Numerical simulations. *J. Climate Appl. Meteor.*, **26,** 1293–1304.

Lunny, R. M., ed., 1959: The voyage of the *Half Moon* from 4 April to 7 November 1609. *Juet's journal,* The New Jersey Historical Society, 37 pp.

Maki, M., and T. Harimaya, 1988: The effect of advection and accumulation of downslope air on nocturnal cooling in basins. *J. Meteor. Soc. Japan,* **66,** 581–597.

Meyer, M. B., and G. G. Lala, 1989: Climatological aspects of radiation fog occurrence at Albany, New York. *J. Climate,* submitted.

——, J. E. Jiusto and G. G. Lala, 1986: FOG-82: A cooperative field study of radiation fog. *Bull. Amer. Meteor. Soc.*, **67,** 825–832.

Monteith, J. L., 1956: Dew. *Quart J. Roy. Meteor. Soc.*, **83,** 322–341.

Musson-Genon, L., 1987: Numerical simulation of a fog event with a one-dimensional boundary layer model. *Mon. Wea. Rev.*, **115,** 592–607.

Nieuwstadt, F. T. M., and R. A. Brost, 1986: The decay of convective turbulence. *J. Atmos. Sci.*, **43,** 532–546.

Oliver, D. A., W. S. Lewellen and G. G. Williamson, 1978: The interaction between turbulent and radiative transport in the development of fog and low-level stratus. *J. Atmos. Sci.*, **35,** 301–316.

Petterssen, S., 1940: *Weather Analysis and Forecasting.* McGraw-Hill, 503 pp.

Pilié, R. J., E. J. Mack, W. C. Kocmond, W. J. Eadie and C. W. Rogers, 1975a: The life cycle of valley fog: Part I–micrometeorological characteristics. *J. Appl. Meteor.*, **14,** 347–363.

——, ——, ——, —— and ——, 1975b: The life cycle of valley fog: Part II–fog microphysics. *J. Appl. Meteor.*, **14,** 364–374.

——, B. J. Wattle, E. J. Mack and J. T. Hanley, 1982: The role of vegetation in the low-level water budget in fog. Fog-82: A cooperative field study of radiation fog. ASRC-SUNY pub. no. 984. [available from Atmospheric Sciences Research Center, 100 Fuller Road, Albany, NY 12205.]

Roach, W. T., and A. Slingo, 1979: A high resolution infrared radiative transfer scheme to study the interaction of radiation with cloud. *Quart. J. Roy. Meteor. Soc.*, **105,** 603–614.

——, R. Brown, S. J. Caughey, J. A. Garland and C. J. Readings, 1976: The physics of radiation fog: Part I–a field study. *Quart. J. Roy. Meteor. Soc.*, **102,** 313–333.

——, ——, ——, B. A. Crease and A. Slingo, 1982: A field study of nocturnal stratocumulus. I. Mean structure and budgets. *Quart. J. Roy. Meteor. Soc.*, **108,** 103–124.

Rodhe, B., 1962: The effect of turbulence on fog formation. *Tellus,* **14,** 49–86.

Samson, P. J., G. Neighmond and A. J. Yencha, 1975: The transport of suspended particulates as a function of wind direction and atmospheric conditions. *J. Air Poll. Control Ass., 25,* **12,** 1232–1237.

Slingo, A., R. Brown and C. L. Wrench, 1982: A field study of nocturnal stratocumulus: Part III–High resolution radiative and microphysical observations. *Quart. J. Roy. Meteor. Soc.*, **108,** 145–165.

Stull, R. B., 1988: *An Introduction to Boundary Layer Meteorology.* Kluwer Academic, 666 pp.

Taylor, G. I., 1917: The formation of fog and mist. *Quart. J. Roy. Meteor. Soc.*, **43,** 241–268.

Turton, J. D., and R. Brown, 1987: A comparison of a numerical model of radiation fog with detailed observations. *Quart. J. Roy. Meteor. Soc.*, **113,** 37–54.

Webb, E. K., 1970: Profile relationships: The log linear range and extension to strong stability. *Quart. J. Roy. Meteor. Soc.*, **96,** 67–90.

Welch, R. M., M. G. Ravichandran and S. K. Cox, 1986: Prediction of quasi-periodic oscillations in radiation fogs. Part I: Comparison of simple similarity approaches. *J. Atmos. Sci.*, **43,** 633–651.

Wyngaard, J. C., 1975: Modelling the planetary boundary layer–extension to the stable case. *Bound.-Layer Meteor.*, **11,** 89–102.